Nucleic Acids Research, 2021 **1**
https://doi.org/10.1093/nar/gkab770

A rapid method to visualize human mitochondrial DNA replication through rotary shadowing and transmission electron microscopy

Martin Kosar[1], Daniele Piccini[1], Marco Foiani[1,2,*] and Michele Giannattasio[1,2,*]

[1]IFOM, Fondazione Istituto FIRC di Oncologia Molecolare, Milano, Italy and [2]Dipartimento di Oncologia & Emato-Oncologia, Università degli Studi di Milano, Milano, Italy

Received March 05, 2021; Revised August 15, 2021; Editorial Decision August 22, 2021; Accepted August 26, 2021

ABSTRACT

We report a rapid experimental procedure based on high-density *in vivo* psoralen inter-strand DNA cross-linking coupled to spreading of naked purified DNA, positive staining, low-angle rotary shadowing, and transmission electron microscopy (TEM) that allows quick visualization of the dynamic of heavy strand (HS) and light strand (LS) human mitochondrial DNA replication. Replication maps built on linearized mitochondrial genomes and optimized rotary shadowing conditions enable clear visualization of the progression of the mitochondrial DNA synthesis and visualization of replication intermediates carrying long single-strand DNA stretches. One variant of this technique, called denaturing spreading, allowed the inspection of the fine chromatin structure of the mitochondrial genome and was applied to visualize the *in vivo* three-strand DNA structure of the human mitochondrial D-loop intermediate with unprecedented clarity.

INTRODUCTION

The human mitochondrial genome is constituted by a circular double-strand DNA (dsDNA) molecule of ∼16.6 kb (1).

Based on its content in DNA bases, one filament of the mitochondrial DNA is defined as heavy strand (HS), while the complementary strand is the light strand (LS). The HS and LS filaments are replicated from two spatially separated DNA replication origins located, respectively, in the major non-coding region (heavy strand replication origin- OH) or in a short intergenic spacer (light strand replication origin-OL) of the mitochondrial genome (Figure 1) (2–5).

Three main modes were proposed for the replication of the human mitochondrial DNA: the Strand Displacement Model (SDM) (5–14), the RNA Incorporated Through-Out the Lagging Strand (RITOLS) (15–22) model, and the Strand Coupled Mechanism (SCM) (15,23) (Figure 1). The relative frequency of *in vivo* utilization of these three mechanisms, their regulations, and reciprocal inter-connections remain mainly unknown. While the SDM and RITOLS imply the presence of spatially and temporally separated HS and LS polymerization activities, the SCM entails the synchronous progression of the HS and LS DNA synthesis and the existence of a mitochondrial DNA replication bubble (also called theta intermediate) and it appears to be a replication mode utilized only in certain specific conditions (Figure 1) (24–28).

It has been shown that ∼95% of the HS DNA synthesis initiation events terminate at the Termination Associated Sequences (TAS) located around 650 nt downstream of the heavy strand DNA replication origin (OH), leading to the formation of circular mitochondrial DNA molecules carrying a short D-loop (Figure 1A, B) (29). This structure consists of the triple-stranded DNA bubble in the major Non-Coding Region (NCR) of the human mitochondrial DNA, which was identified in early pioneering studies (Figure 1A and B) (6,7,29). How and when the arrested HS DNA synthesis is re-started from the short D-loop remains mainly unknown, although possible molecular mechanisms have been recently proposed (30).

Besides the dynamics of D-loop formation and re-start, the exact molecular mechanisms, cellular feedbacks, and physiological conditions that promote or inhibit extended mitochondrial DNA replication (and regulate mitochondrial DNA copy number) are not completely understood. For example, it has been shown that depletion of mitochondria induced by certain experimental conditions can cause activation of extended mitochondrial DNA replication (23,31).

During the SDM of replication, the progression of the newly synthesized HS displaces the parental HS leading to the formation of a circular molecule carrying an extended D-loop with a long stretch of single-stranded DNA (ssDNA). The length of ssDNA can reach two-thirds of

*To whom correspondence should be addressed. Tel: +39 02574303307; Email: michele.giannattasio@ifom.eu
Correspondence may also be addressed to Marco Foiani. Email: marco.foiani@ifom.eu

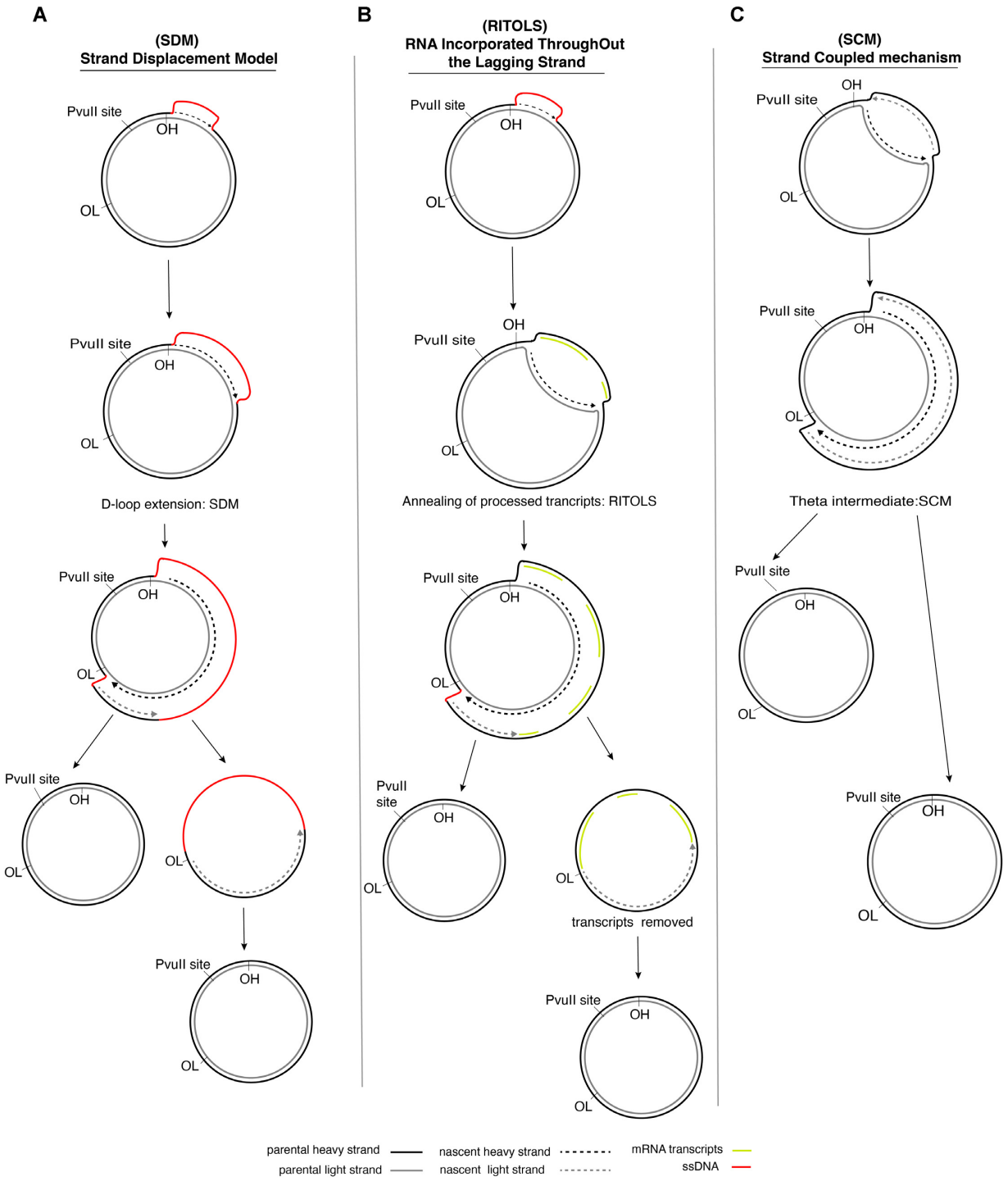

Figure 1. Three main models for human mitochondrial DNA replication. (**A**) The Strand Displacement Model (SDM). HS replication starts from the OH and displaces the parental HS until the OL origin is reached by the newly synthesized HS. The LS replication starts when around two-thirds of the HS replication is completed. Following the completion of the HS replication, a fully replicated mitochondrial genome is released (composed of a parental light strand and a newly synthesized heavy strand) together with a gapped circle (composed of a parental heavy strand and an incompletely newly synthesized light strand) due to incomplete LS DNA synthesis. Completion of LS synthesis will create the second fully replicated mitochondrial genome composed of the parental heavy strand and the completely newly synthesized light strand. (**B**) RNA Incorporated Throughout the Lagging Strand (RITOLS). The RITOLS model is similar to the SDM, and it also implies spatially and temporally separated HS and LS DNA synthesis events. The RITOLS model predicts that processed ssRNA messengers anneal to the displaced parental HS leading to the formation of replication bubbles composed of two filaments, constituted, respectively, of dsDNA and ssDNA/ssRNA (i.e., DNA:RNA hybrids). As in SDM, the completion of the HS synthesis in RITOLS will create a fully replicated genome as well as the advancement of LS DNA synthesis will remove the annealed mRNAs (processed transcripts) from the HS, which will be replaced by the newly synthesized LS strand leading to the creation of the second fully replicated mitochondrial genome. (**C**) The strand coupled mechanism (SCM) implies a simultaneous advancement of HS and LS DNA synthesis and the presence of a classical DNA replication bubble composed of two dsDNA filaments (also called theta intermediate).

the mitochondrial genome's length (Figure 1A) (8). This long stretch of ssDNA was recently shown to be bound by the mitochondrial ssDNA-binding protein (mtSSB) *in vivo* (32), although the full coverage of the displaced HS filament by the mtSSB cannot be assessed at the level of single mitochondrial DNA molecules using ChIP-seq-based approaches. Another *in vitro* study refers that mtSSB does not display cooperative binding to ssDNA (33).

In the SDM, when the light strand replication origin (OL) is reached by the newly synthesized HS, it gets activated, leading to the initiation of the LS DNA replication (Figure 1A) (32,34). HS replication will then proceed until a fully replicated mitochondrial DNA molecule is released together with a circular molecule carrying a ssDNA gap due to incomplete LS strand DNA replication (gapped circle) (Figure 1A).

The completion of the LS replication (gap-filling of the gapped circle) will generate a second fully replicated mitochondrial DNA molecule leading to the completion of mitochondrial DNA replication. The RITOLS model predicts that the displaced parental HS does not remain single-stranded, but it anneals with processed mRNA transcripts, leading to the formation of a circular molecule carrying a four-strand DNA bubble with one side of the bubble composed of one newly synthesized HS annealed to a parental LS filament and the other side of the bubble composed of the displaced parental HS annealed to an RNA filament (processed transcript) leading to the formation a theta-like structure carrying RNA tracks (Figure 1B) (16,19,21).

During RITOLS, the completion of the HS DNA synthesis will release a fully replicated mitochondrial DNA molecule. In contrast, the advancement of the LS DNA synthesis will lead to the replacement of the annealed transcripts from the parental HS, creating the second fully replicated mitochondrial DNA molecule (Figure 1B). The enzymology and dynamic of the removal of those annealed RNA filaments from the displaced HS are not known. During RITOLS, the existence of additional initiation sites for the LS DNA replication has been proposed besides the already established OH and OL initiation sites mapped in early pioneering experiments (3,4,13,18,23,35,36). Both SCM and RITOLS entail, respectively, the existence of classic DNA replication bubbles composed of two ds-DNA filaments or a bubble with one dsDNA filament and one DNA:RNA filament (i.e., DNA/RNA hybrid) (Figure 1B, C). Both intermediates are defined as theta structures.

During the SCM of replication of the mitochondrial genome, there is a synchronous and opposite advancement of the HS and LS DNA synthesis, or, alternatively, coupled leading/lagging strand replisomes carry on the replication of the mitochondrial genome. SCM has been reported to be a backup replication mode activated in specific conditions (Figure 1C) (15,18,23,31).

Deep insights into the mechanism of replication of the mitochondrial DNA came from the utilization of the Kleinschmidt spreading technique (protein-based spreading method) (37,38) coupled to rotary shadowing (39) and Transmission Electron Microscopy (TEM) to analyze mitochondrial DNA purified from the genomic DNA through caesium chloride or other density gradient-based techniques (6,8,40–42). Also neutral-neutral 2D gel electrophoresis is instrumental to the study of the mechanics and dynamics of mitochondrial DNA replication (43). Although these workflows remain the 'gold standard', density gradient-based purification of the mitochondrial DNA requires a long operator time, complex instruments (e.g., ultracentrifuges), extensive usage of chemicals, and it is not suitable for the quick analysis of multiple mitochondrial DNA samples. Moreover, in the protein-based method of DNA spreading (38), a complex between DNA and denatured cytochrome C at the air-hypo-phase interface is visualized through TEM, which does not allow clear visualization of the ssDNA stretches on the DNA molecules. In addition, the protein-based spreading method cannot be utilized for the denaturing spreading technique (see the following paragraphs and Materials and Methods).

Here we modified and optimized a well-established protocol originally designed for the analysis of the chromosomal DNA replication intermediates using Transmission Electron Microscopy (TEM) (44–48) and adapted it for the rapid visualization of human mitochondrial DNA replication. Two main modifications were introduced to this well-established procedure at the level of the *in vivo* psoralen-mediated inter-strand DNA cross-linking and mitochondrial DNA extraction. The presented approach to visualize mitochondrial DNA replication takes advantage of high-density *in vivo* psoralen-mediated inter-strand DNA cross-linking, optimized rapid DNA extraction, and the procedure to enrich the ssDNA containing DNA replication intermediates (46,47). A well-established benzyl-dimethyl-alkyl-ammonium chloride (BAC)-based spreading procedure of naked, highly purified DNA combined with optimized low-angle rotary shadowing with platinum and Transmission Electron Microscopy (TEM) are then utilized to visualize HS and LS mammalian mitochondrial DNA replication. Importantly, the specific spreading and low-angle rotary shadowing conditions (using highly controlled electron beam evaporation) allow to clearly distinguish the difference between dsDNA and ssDNA, thus providing unprecedented clarity for the structural studies of mitochondrial DNA replication intermediates (49,50).

Besides that, we used the variant of this technique called 'denaturing spreading' (45,46,48), which allows for the detailed inspection of the chromatin structure (nucleosome positioning) and more precise analysis of the DNA structures. In particular, the denaturing spreading technique was utilized to visualize the *in vivo* three-stranded structure of the short human mitochondrial D-loop.

In summary, the structural analysis of linearized human mitochondrial genomes (through the use of specific replication maps) allows clear and quick visualization of the progression of the heavy strand (HS) human mitochondrial DNA replication. The fine chromatin structure of the mitochondrial genome can be inspected in detail with the denaturing spreading technique, and the high density of *in vivo* DNA inter-strand cross-links prevents the formation of artifacts during the purification of the mitochondrial genome. The evidence presented here is in good agreement with the uncoupled models of mitochondrial DNA replication, which entails the spatial and temporal separation of HS and LS DNA synthesis.

MATERIALS AND METHODS

In vivo psoralen-mediated inter-strand DNA cross-linking

U-2 OS (ATCC) and HeLa cells (European Collection of Authenticated Cell Cultures: ECACC) were grown in Dulbecco's Modified Eagle's Medium (Sigma-Aldrich, #D6171) supplemented with Fetal Bovine Serum (Sigma-Aldrich, #F7524) to a final concentration of 10%. BJ cells (ATCC) were grown in Minimum Essential Media (Biowest, #L0440) supplemented with Fetal Bovine Serum (Sigma-Aldrich, #F7524) to a final concentration of 10%. In total, 22 million cells grown in four 15 cm diameter dishes (80% confluency) were used for each EM sample. Before the experiment, each dish was washed with 20 ml of 1x Phosphate Buffered Saline (PBS), and cells were trypsinized using 1.5 ml of trypsin-EDTA solution for 10 minutes. Next, 10 ml of DMEM were added to the detached cells, and cells from the four dishes were collected into a single 50 ml falcon tube resulting in a total volume of ∼46 ml (=1 EM sample). From now on, cells were kept on ice, and the subsequent steps of the protocol until the cell lysis were carried on rapidly. Cells were spun down at 290 g for 5 min at 4°C, and the residual DMEM was carefully removed using a 1000 μl pipette tip. The cellular pellet was resuspended in 5 ml of cold 1× PBS (4°C). The cell suspension was transferred into a 15 ml falcon tube (1 tube/sample), and cells were again spun down at 290 g for 5 min at 4°C. The residual PBS was carefully removed using a 1000 μl pipette tip, and the cellular pellet corresponding to each sample was gently resuspended in 3 ml of 1× PBS.

Next, cells from each sample were transferred into an open 6 cm diameter dish with a stirring bar inside. The 6 cm dish was then placed into a 10 cm diameter dish (without the lid) containing ice on the bottom and the sides of the dish. This setup is critical to keep the cells constantly on the ice during the incubation and UVA irradiation cycles. Therefore, the ice was replaced once it dissolved during the irradiation cycles. The dishes with the cells were placed on a mini-magnetic stirrer, and the cells were continuously mixed. Next, 50 μl of 4,5′,8-Trimethylpsoralen (TMP) (2mg/ml stock concentration prepared in DMSO; stored at −20°C in the dark; Sigma-Aldrich, #T613) were added to each 6 cm dish. Cells covered with aluminum foil to prevent light exposure were incubated under magnetic stirring on ice for 5 min. After that, cells were placed into a Stratalinker UV Crosslinker Model 1800 (Stratagene, #400072) with an irradiation chamber equipped with monochromatic 365 nm bulbs (8 W bulbs, 5 bulbs) and irradiated for 5 min. The UVA chamber's irradiance was measured as previously described so that a defined and reproducible irradiation energy was delivered to the samples (46). The cell suspensions were kept at no more than 2–3 cm from the UVA bulbs. Adding of the fresh TMP, 5 min incubation in the dark, and 5 min irradiation cycles were repeated three times (four cycles in total). Irradiation of the cells with UVA in the presence of psoralen will induce the formation of DNA inter-strand cross-links. These specific conditions of *in-vivo* DNA inter-strand cross-linking are specifically optimized to induce the formation of a high-density of covalent cross-links between the opposing adjacent DNA bases on the antiparallel filaments of the DNA molecule. In particular, in these experimental conditions, the linkers regions between nucleosomes will be cross-linked with high efficiency leading to the creation of covalent links in more than 90% of the linker regions between nucleosomes (see the text of the manuscript) and (46). After the last irradiation cycle, the cell suspension was transferred into a 15 ml falcon tube. In addition, dishes were washed twice with additional 4 ml of cold 1× PBS to ensure that all cells were collected from the dishes. The collected cell suspension had a volume of around 11.2 ml/sample.

DNA extraction

Following the psoralen-mediated DNA inter-strand cross-linking (the step above), 15 ml falcon tubes with cells were spun down at 290 g for 5 min at 4°C. Residual PBS was carefully removed from the cell pellet using a 1000 μl pipette tip. Each sample's cellular pellet was resuspended in 3 ml of TNE buffer (10 mM Tris–HCl, pH 7.4; 100 mM NaCl; 10 mM EDTA; room temperature). 10 μl of Ribonuclease A (RNase A) (10 mg/ml stock concentration dissolved in distilled sterile H_2O and prepared with the 'boiling method' as described in Maniatis *et al*. 1982; RNase A Sigma-Aldrich, #R5000) were added to each sample. Next, 3 ml of TNES buffer (TNE buffer + 1% sodium dodecyl sulfate (SDS), at room temperature) were added, and cells were resuspended using a 1000 μl pipette tip with a cut end. Samples were incubated at 37°C for one hour in a water bath to allow complete digestion of RNA species by the RNase A and initiation of the cells lysis due to the presence of SDS. Next, 50 μl of Proteinase K solution were added (10 mg/ml stock concentration in dH_2O; Roche, #3115887001), and the cell suspension was mixed four times using 1000 μl pipette tip placed on 5 ml plastic pipette. Samples were incubated overnight in a water bath at 37°C to allow complete cell lysis and extensive digestion of proteins by Proteinase K.

The next day, total DNA (containing both genomic and mitochondrial DNA) was extracted by adding 6 ml (corresponding to one volume) of phenol: chloroform:isoamyl alcohol (25:24:1 Sigma-Aldrich, #P2069). Samples were vigorously mixed by reverting the falcon tubes for 30 sec and spun down at 3220 g for 5 min at room temperature. Next, 5 ml of the upper water phase (clear) containing DNA were transferred to a new 15 ml falcon tube. 5 ml (one volume) of chloroform (Sigma-Aldrich, #372978) were added to remove traces of the phenol from the previous step. Samples were mixed vigorously by inverting the falcon tubes for 30 sec and spun down at 3220 g for 5 min at room temperature. 5 ml of the upper water phase (clear) containing DNA was transferred to a new 15 ml falcon tube. 500 μl of 3 M sodium acetate pH 5.5 (1/10 of the total volume) were added, and the solution was mixed 20 times using a 5 ml plastic pipette. Next, 5.5 ml of 2-propanol (VWR, #20842.330) (one volume) were added, and the solution was mixed by inverting the falcon tube for 20 sec until the white stripes of precipitated DNA appeared. The precipitated DNA was moved to a 1.5 ml microcentrifuge tube with 1 ml of 70% ethanol (VWR, #20821.330) using a 1000 μl pipette tip (or mono-use plastic loops) and spun down at 16 000 g for 3 min at 4°C. Traces of ethanol were removed. The pellet with the DNA was washed with 1 ml of ethanol 70% and spun down

for 5 min at 16 000 g at 4°C. Traces of the ethanol were removed from the pelleted DNA, and the tube with the DNA pellet was left open for ∼15 min until completely dried. Finally, DNA was dissolved in 300 μl of 10 mM Tris–HCl, pH 8.0 and gently mixed until completely dissolved. The DNA samples were stored at 4°C to prevent damage to the chromosomal and mitochondrial DNA intermediates, which can occur in the case of repeated cycles of freezing the samples at −20°C.

DNA digestion

As the protocol applies to pure DNA (46), it is advisable to confirm the purity of the genomic DNA preparation by checking the absorbance ratios (260/280 nm = 1.8 indicates pure DNA; 260/280 nm = 2.0 indicates pure RNA). Usually, pure DNA preparations give a ratio of 260/230 nm of around 2.0–2.2. If the pure DNA is resuspended in slightly basic conditions (pH 8.0), this ratio 260/280 can increase by 0.2–0.3 units, while if resuspended in slightly acidic conditions (pH 6.5), the value of the ratio will decrease by 0.2–0.3.

Typically, around 10–25 μg of highly pure genomic DNA is digested for the EM sample preparation. It is recommended to use quantification methods, which directly measure genomic DNA concentration, such as serial dilutions of the DNA loaded on an agarose gel together with known DNA standards, or the Qubit fluorometer-based protocol. If DNA preparations contain RNA, DNA concentration analysis with the Nanodrop spectrophotometer could give an over-estimated read of the DNA concentration.

Using the psoralen-mediated cross-linking conditions indicated in the previous step, around 70–100 units of PvuII-HF enzyme (New England Biolabs, #R3151S) are sufficient to obtain digestion of 10–15 μg of genomic DNA (7–10 units/μg of genomic DNA) in three to five hours at 37°C. The total volume of digestion is usually 250 μl. If it is possible to retain the restriction enzyme's efficiency, it is advisable to use digestion buffers that do not contain Bovine Serum Albumin (BSA), which can stick to the purified DNA fibers during the enrichment process and contaminate the DNA samples for the electron microscopy analysis. After the digestion, if the genomic DNA contains traces of dsRNA, 1 μl of RNase III (New England Biolabs, #M0245S) (2 units/μl diluted 1:100 in autoclaved sterile Milli-Q water) can be added to the digestion mix for 30–60 min at 37°C to digest dsRNA completely. This step is not necessary if the genomic DNA preparation does not contain dsRNA.

Analysis of non-enriched DNA samples

To analyze the non-enriched DNA samples (= samples in which BND-cellulose/G20 column enrichment procedures were omitted), upon completion of the digestion of the genomic DNA with PvuII-HF (see the previous paragraph), an aliquot containing 1–5 μg of digested genomic DNA is taken from the digestion mix. The digested DNA is subjected to two extractions with the same volume of chloroform (Sigma-Aldrich, #372978) to remove the traces of the restriction enzyme that could stick to the DNA fibers. After the second extraction with chloroform, the aqueous phase is separated from the organic phase, and the digested genomic DNA is precipitated using a classic Sodium Acetate/Ethanol precipitation. The precipitated DNA is resuspended in 500 microliters of Tris–HCl 10 mM, pH 8 and subjected to purification through the Amicon Ultra-0.5 ml Centrifugal Filters (100K, Millipore, #C82301) as described in the following paragraphs of the Materials and Methods. 10–50 ng of the precipitated and purified DNA are subjected to the spreading technique described in the following paragraphs of the Materials and Methods. The EM grids with the non-enriched genomic DNA adsorbed on the carbon surface are subjected to the low-angle rotary shadowing with 8 nm of platinum as described in the following paragraphs of the Materials and Methods. EM pictures have been acquired as described in the following paragraphs of the Materials and Methods.

Enrichment of the ssDNA containing mitochondrial DNA replication intermediates

Preparation of the BND-cellulose stock suspension for the BND-cellulose columns. The benzoylated naphthoylated diethyl aminoethyl (DEAE)-cellulose (from now on BND-cellulose) stock was prepared by dissolving BND-cellulose granules (Sigma-Aldrich, #B6385, concentration 0.1–0.5 g/ml, depending on the BND-cellulose batch) in 30 ml of buffer containing 10 mM Tris–HCl, pH 8.0 and 300 mM NaCl in a 50 ml falcon tube. The BND-cellulose clumps were dissolved by extensive vortexing and vigorous pipetting using 5 ml plastic pipettes and a cut 1000 μl pipette tip. The concentration of BND-cellulose granules into the stock solution can vary (0.1–0.5 g/ml) depending on the dimension of the BND-cellulose particles in the BND-cellulose batch. The BND-cellulose resin suspension was centrifugated at 3197 rcf for 5 min at 4°C. After the centrifugation, the supernatant was discarded using a 5 ml plastic pipette, and the resin was washed four times in 30 ml of buffer containing 10 mM Tris–HCl, pH 8.0 and 300 mM NaCl. In some of the BND-cellulose batches, a consistent amount of BND-cellulose resin may remain in the supernatant, likely due to the presence of a fraction of small dimension particles in the BND-cellulose preparation. Also, a sort of white emulsion can be seen on the surface of the supernatant solution due to the saponification process utilized for BND-cellulose production. Properly dissolved and washed BND-cellulose stock must appear as a homogeneous suspension without clamps, granules, or emulsions. Typically, 5 ml of the stock solution were prepared and stored at 4°C for 1–2 months. The stock was resuspended by vortexing and pipetting to prepare a homogeneous suspension before preparing the BND-cellulose column bed as described in the following step.

Preparation of the BND-cellulose columns. Next, mono-use Poly-Prep chromatography columns (Bio-Rad, #7311550) were utilized. 1–3 ml of BND-cellulose stock suspension were applied to the chromatographic column. Depending on the BND-cellulose batch, the volume of BND-cellulose stock that needs to be applied to the column can vary. The BND-cellulose resin was allowed to get packaged into the column through gravity flow. The height of the BND-cellulose bed in the column should be around 1–2 cm. The flow rate can vary for different

BND-cellulose batches, likely because of the various dimensions of the BND-cellulose particles. To wash the columns, 1 ml of buffer (filtered through 0.2 μm Millipore filter) containing 10 mM Tris–HCl, pH 8.0 and 1 M NaCl was added, and the resin was resuspend using 2 ml plastic pipettes. Buffer was allowed to pass-through the resin completely, and the wash was repeated six times in total. Next, columns were washed six times using the second buffer (filtered through 0.2 μm Millipore filter) containing 10 mM Tris–HCl, pH 8.0 and 300 mM NaCl. After the last wash, the column was left with 1 ml of buffer (10 mM Tris–HCl, pH 8.0; 300 mM NaCl), and the yellow bottom cap was closed. At this point, BND-cellulose columns are ready to be utilized for the enrichment process of ssDNA containing DNA replication intermediates. Importantly, columns containing BND-cellulose were not allowed to dry out.

Enrichment of the DNA replication intermediates using BND-cellulose. After the DNA digestion, 32.76 μl of autoclaved Milli-Q water, 300 μl of the buffer containing 10 mM Tris–HCl (pH 8.0) and 300 mM NaCl, 17.24 μl of the buffer containing 5 M NaCl were added to the DNA digestion mix to obtain the final volume of 600 μl and to adjust the NaCl concentration. Next, the DNA digestion mix was loaded on the BND-cellulose column prepared and equilibrated with the buffer containing 10 mM Tris–HCl, pH 8.0 and 300 mM NaCl. The buffer used to equilibrate the column was completely eliminated by the gravity flow, and the bottom of the column was closed with the cap. The DNA digestion mix was immediately applied to the BND-cellulose column without letting the column dry. 2 ml plastic pipettes were used to gently resuspend the BND-cellulose resin together with the DNA digestion mix. The digestion mix was incubated with the BND-cellulose for 30 min at room temperature to allow a full binding of DNA molecules to the resin. BND-cellulose resin bed was gently resuspended every 5 min using a sterile 2 ml plastic pipette, avoiding extensive pipetting as it can damage the DNA intermediates.

After the incubation, the cap was removed, and the DNA digestion mix was allowed to pass through the BND-cellulose column. This fraction was collected as a 'Flow-through' for the follow-up analysis. The column was then washed two times with 1 ml of filtered wash buffer containing 10 mM Tris–HCl, pH 8.0 and 1M NaCl. The resin was gently resuspended using 2 ml plastic pipettes after adding the wash buffer, and the column was completely emptied before an additional wash. These fractions, containing mainly linear double-stranded DNA molecules, were collected in 2 ml microcentrifuge tubes marked as a 'Salt fraction' for the follow-up analysis. Next, the BND-cellulose column was closed using the bottom cap, and 600 μl of freshly prepared and filtered (0.2 μm Millipore filter) buffer (caffeine solution) containing 10 mM Tris–HCl (pH 8.0), 1 M NaCl, 1.8% caffeine (weight/volume, Sigma-Aldrich, #C0750) was applied to the BND-cellulose column to elute the DNA replication intermediates carrying ssDNA stretches. It is important that the caffeine solution does not contain caffeine crystals, and it should be freshly prepared and filtered before use. The BND-cellulose resin was incubated for 30 min with the caffeine solution and was gently resuspended (using 2 ml plastic pipettes) each 5 min. The column's cap was removed, and the solution containing DNA replication intermediates carrying ssDNA stretches was collected into sterile 1.5 ml microcentrifuge tubes marked as a 'Caffeine fraction'. The tubes were spun down at 16 000 rcf for 5 min at room temperature. After the centrifugation, the caffeine fractions were transferred into new sterile 1.5 ml microcentrifuge tubes without touching the pellet containing the residual BND-cellulose particles. This centrifugation step was added to avoid the carryover of BND-cellulose particles in the final EM samples. At this point, the caffeine fractions containing the DNA replication intermediates carrying ssDNA can be further purified following two alternative procedures: Amicon Ultra-0.5 ml Centrifugal Filters or classic isopropanol/potassium acetate precipitation.

Purification of the DNA replication intermediates obtained using the BND-cellulose columns. The fractions obtained in the previous steps were immediately passed through Amicon Ultra-0.5 ml Centrifugal Filters (100K, Millipore, #C82301) to remove the excess of caffeine and high salt concentration in the elution buffer. The Amicon Ultra-0.5 ml Centrifugal Filters for the 'Flow-through', 'Salt fraction' and 'Caffeine fraction' were assembled according to the manufacturer's protocol. Amicon filters were then hydrated and equilibrated with 500 μl of 10 mM Tris–HCl, pH 8.0. Next, 500 μl of the collected fractions were loaded on the equilibrated filters and spun down at 5000 g for 10 min at room temperature. After the centrifugation, the liquid in the collection tubes was discarded, and the filters were washed with 500 μl of 10 mM Tris–HCl, pH 8.0, followed by the centrifugation at 5000 g for 10 min at room temperature. The wash of the collected fractions was repeated three more times (four washes in total). After the last wash, the liquid in the collection tube was discarded, the Amicon filter was transferred upside down into a new collection tube provided by the manufacturer and spun down at 1000 g for 1 min at room temperature. Purified DNA intermediates were transferred from the collection tube into a sterile 1.5 ml microcentrifuge tube. The final volume of the recovered DNA sample ('Caffeine fraction') should be around 15–25 μl. Extensive pipetting of the sample should be avoided to prevent damage to the DNA replication intermediates. Small aliquots of the fractions were loaded on the agarose gel to estimate the efficiency of the enrichment process.

Enrichment of the DNA replication intermediates using QIAGEN Genomic-tip 20/G anion-exchange columns. Alternatively, ssDNA containing DNA replication intermediates can be enriched using the QIAGEN Genomic-tip 20/G anion-exchange columns instead of the BND-cellulose columns. This protocol replaces the BND-cellulose-based enrichment procedure (see the previous paragraphs of Materials and Methods). Following the DNA digestion (see the paragraph above of the Materials and Methods), the volume of the digestion mix was adjusted to 1 ml using the buffer containing 10 mM Tris–HCl, pH 8.0 and 300 mM NaCl. QIAGEN Genomic-tips 20/G (Qiagen, #10223) columns were equilibrated with 1 ml of QBT buffer (50 mM Mops pH 7.0, 750 mM NaCl, 15% isopropanol (v/v), 0.15%

Triton X-100 (v/v) (Qiagen, #19054)) for 5 min (46). Next, the QIAGEN Genomic-tips 20/G columns were washed three times with 2 ml of the buffer containing 10 mM Tris–HCl (pH 8.0), 1 M NaCl, and three times with 1 ml of the buffer containing 10 mM Tris–HCl (pH 8.0) and 300 mM NaCl. Both buffers were filtered through 0.2 μm Millipore filters. After the wash, the bottom of the QIAGEN Genomic-tip 20/G column was closed with a cap, and 1 ml of the previously adjusted digestion mix was loaded on the QIAGEN Genomic-tip 20/G column and incubated for 10 min at room temperature to allow binding of the DNA to the column. After the incubation, the cap was removed, and the DNA digestion mix was allowed to pass through the QIAGEN Genomic-tip 20/G column and collected into a 1.5 ml microcentrifuge tube as a 'Flow-through' for the follow-up analysis. Next, the QIAGEN Genomic-tip 20/G column was washed twice with 1 ml of filtered buffer containing 10 mM Tris–HCl (pH 8.0), 1 M NaCl, and the wash buffer passed through the column was collected into a 1.5 ml microcentrifuge tube as a 'Salt fraction' for the follow-up analysis.

This fraction should contain mostly linear dsDNA molecules without DNA replication intermediates. To elute the ssDNA containing DNA replication intermediates, 600 μl of freshly prepared and filtered (0.2 μm Millipore filter) buffer containing 10 mM Tris–HCl (pH 8.0), 1 M NaCl, 1.8% caffeine (weight/volume, Sigma-Aldrich, #C0750) were applied to the QIAGEN Genomic-tip 20/G column and incubated 15 min at room temperature to allow complete elution of the ssDNA containing DNA replication intermediates. The elution fraction was collected into sterile 1.5 ml microcentrifuge tubes marked as a 'Caffeine fraction'. Next, an additional 600 μl of the elution caffeine solution was applied to the QIAGEN Genomic-tip 20/G column, which was incubated for 5 min at RT, and the elution buffer was collected into the same 1.5 ml microcentrifuge tubes as previously indicated to increase the yield in DNA replication intermediates containing ssDNA. The purification of the Caffeine fraction containing the DNA replication intermediates was performed using Amicon Ultra-0.5 ml Centrifugal Filters (100K, Millipore, #C82301) according to the same protocol as for the purification of the fractions derived from the BND-cellulose enrichment procedure (see the paragraphs above of Materials and Methods).

Electron microscopy analysis

Native spreading. For the native spreading, a mix of the DNA sample ('Caffeine fraction' or 'non-enriched DNA', both purified on Amicon Ultra-0.5 ml Centrifugal Filters, see the previous paragraphs of Materials and Methods), formamide (Merck #F9037) and the solution of the detergent BAC (Sigma-Aldrich, #12060) was prepared. First, BAC powder was dissolved to 0.2% (w/v) in formamide (Merck #F9037) and then diluted 1:10 in 10 mM Tris–HCl, pH 8.0 to obtain the BAC stock solution. Next, 5 μl of formamide (Merck #F9037) and 0.4 μl of BAC stock solution were deposited on the bottom of a 1.5 ml microcentrifuge tube (46), creating the spreading mix. 5 μl of enriched ('Caffeine fraction') or non-enriched DNA samples resuspended in 10 mM Tris–HCl, pH 8.0 to the final concentration of 10–50 ng/μl were added to the spreading mix without pipetting.

Immediately after that, 8 μl of the spreading mix were deposited on the surface of a mica glass sheet and allowed to slide down on the glass and to get in contact with the water surface (hypo-phase) previously created by adding 30-50 ml of the nuclease-free AccuGene Molecular Biology Water (Lonza, #BE51200) to a 15 cm diameter plastic dish as previously described (46). Thanks to the presence of the BAC, once the drop of the spreading mix touches the water surface (hypo-phase), a mono-molecular layer of DNA molecules is created on the surface of the water. The 'spreading effect' on the big surface of the water (hypo-phase) will lead to the creation of a mono-molecular layer of well-separated and non-overlapping DNA molecules floating on the surface of the water. At the same time, the presence of the formamide creates a slightly denaturing environment that does not impact the structure of the DNA molecules but forces them to acquire an extended conformation. The 'spreading effect' and the presence of formamide prevent the formation of bundles of DNA fibers and create an ideal configuration to analyze the fine ultra-structure of the DNA molecules through TEM.

Denaturing spreading. For the denaturing spreading, 5 μl of the DNA sample ('Caffeine fraction' or non-enriched DNA sample purified on Amicon Ultra-0.5 ml Centrifugal Filters, see previous paragraphs of the Materials and Methods), 5 μl of the formamide, and 0.2 μl of glyoxal solution, 40% (w/v) (8.8 M) of glyoxal dissolved in water (Sigma-Aldrich, #50649), were mixed (without pipetting) creating the denaturing spreading mix, which was incubated for 25 min in a thermomixer set at 42°C. Subsequently, the denaturing spreading mix was chilled on ice for at least for 10 min. During the incubation at 42°C, the two DNA filaments of the DNA double helix become completely denatured except for the points where the opposing adjacent DNA bases on the two antiparallel filaments of the DNA helix were cross-linked *in vivo* by the UVA and psoralen-mediated DNA inter-strand cross-linking procedure (see the previous paragraphs of Material and methods). Next, 0.4 μl of BAC stock solution (see the previous paragraph in Materials and Methods), were added to the denaturing spreading mix immediately before the spreading, which was performed as described in the above paragraph for the native spreading.

Immediately after the spreading of the DNA molecules on the water surface (hypo-phase), either for the native or for the denaturing spreading, the mono-molecular layer of DNA molecules on the surface of the water was touched with a 400-mesh copper TEM grid on which a thin (4–8 nm), homogeneous and low grain carbon layer was deposited (46). The carbon layer utilized for this technique was incubated for 30 min with the ethidium bromide solution immediately before the absorption of the DNA molecules on it. The ethidium bromide stock solution (10 mg/ml dissolved in water, Sigma-Aldrich, #E1510) was filtered (0.2 μm) and subsequently diluted 1:10 in filtered (0.2 μm) nuclease-free AccuGene Molecular Biology water (Lonza, #BE51200) and utilized as described (46) to treat the carbon layer deposited on the electron microscopy grids. This treatment of the surface of the carbon with ethidium

bromide is essential to maximize the efficiency of the adsorption of the DNA molecules on the surface of the carbon without the need of glow discharging it. After the absorption of the DNA molecules on the carbon surface, the electron microscopy grid was immediately submerged into a solution of ethanol and uranyl acetate (Fluka, #73943) as previously described (46).

The 5 mM uranyl acetate stock solution was prepared in filtered (0.2 μm) AccuGene Molecular Biology Water (Lonza, #BE51200) in 5 mM HCl. Since the uranyl acetate has only mild radioactivity (0.37–0.51 μCi/g), the use of the standard protective equipment (gloves, lab coat, glasses) is sufficient to work safely. Next, the uranyl acetate stock solution was diluted 1:10 in 100% ethanol immediately before use. Immediately after touching the spreading surface, the electron microscopy grids with adsorbed DNA molecules were instantly submerged in the uranyl acetate/ethanol solution to allow the de-hydration of the DNA fibers on the carbon surface and the completion of the absorption. Besides that, the uranyl acetate positively stains both ssDNA and dsDNA regions, thus enhancing the contrast in TEM and the better visualization of the ssDNA stretches on the DNA fibers. At this point, the electron microscopy grids with adsorbed DNA fibers on the carbon surface can be stored in electron microscopy plastic racks at room temperature; alternatively, the grids can be immediately subjected to low-angle rotary shadowing with platinum as described in the following paragraph.

Low-angle rotary shadowing conditions. The carbon grids with absorbed DNA molecules stained with uranyl acetate were subjected to a precise low-angle rotary shadowing with a layer of 8 nm of platinum as described previously (46). Here, the following equipment was used: Leica MED020 e-beam (electron beam) evaporator equipped with an oil-free deep vacuum system (membrane and turbo-molecular pumps), the EVM030 control unit with two EK030 electron beam evaporation sources (Leica, #16BU007086-T), the QSG100 film thickness monitor (Leica, #16LZ03428VN), the QSK060 Quartz Head (Leica, #16LZ03440VN), the Tiltable Rotary Stage (Leica, #16BU007283T), and the high precision rotation plate PR01 (ThorLabs, USA) for low-angle rotary shadowing. Overall, the protocol combines the positive staining with uranyl acetate and low-angle rotary shadowing, providing high contrast images of the DNA molecules visualized by TEM and the clear distinction between ssDNA and dsDNA thanks to the different thickness of the two fibers in this experimental condition (46). The utilization of the electron beam evaporation to produce low grain and high-quality carbon and platinum layers and the optimization of the low-angle rotary shadowing conditions with platinum are essential to produce high-quality samples with high contrast on the DNA fibers and the capability of clearly distinguish ssDNA from dsDNA.

TEM pictures acquisition. The EM pictures were acquired using an FEI Tecnai 12 G2 spirit Biotwin microscope operated at 120 kilovolts (KV) in TEM bright-field mode, and a side-mounted optical fibered Gatan Orius SC-1000 camera (11 megapixels) was utilized to generate the TEM images. The average thickness of the DNA fiber in this specific experimental condition was distributed around 10 nm. The conversion factor for the calculation of the DNA fiber length was 0.36 nm/base pair and was established through the measurement of the length of plasmid DNA molecules of known dimensions utilized as internal standards. The pixel size was calibrated at each magnification using the GATAN digital micrograph software (see the next paragraph).

SOFTWARE AVAILABILITY

The Gatan Microscopy Suite Software (Gatan, version 2.3.3 64 bit) and the montage plug-in (Gatan, 64-bit version) were utilized to acquire EM pictures with the side-mounted Orius SC-1000 CCD camera (Gatan). EM pictures raw files were saved in dm3 format. The ImageJ (version 2.1.0/1.53C) software (open source) was utilized to analyze the raw EM pictures.

Dot-blot analysis to detect the content of DNA:RNA hybrids in non-enriched and enriched DNA samples

Serial dilutions of psoralen cross-linked genomic DNA (either non-enriched or enriched using BND-cellulose/G20 column enrichment procedures) were prepared in TE. 150 microliters of each dilution were spotted on Hybond N + membrane (Merck, #GERPN203B), previously equilibrated with TE, using a Bio-Dot SF microfiltration apparatus (Bio-Rad, #1706542) following manufacturer instructions. The Hybond N + membrane was washed with 200 μl of TE and exposed to UV light at 254 nm (Stratalinker UV Crosslinker Model 1800, 8 W bulbs, 5 bulbs, Stratagene, #400072) using the auto-crosslinking function to cross-link the DNA to the membrane. The membrane was washed with 10 mM Tris–HCl, pH 8 and blocked with blocking solution (5% weight/volume powder milk dissolved in 10 mM Tris–HCl, pH 8.0 for 1 h at room temperature (RT)).

The presence of DNA:RNA hybrids in the DNA molecules immobilized on the Hybond N + membrane was detected using the S9.6 antibody diluted in blocking solution. Next, the membrane was washed six times with 10 mM Tris–HCl, pH 8.0, and incubated with a Goat anti-Mouse IgG secondary antibody conjugated with Horseradish Peroxidase (HRP) diluted in blocking solution for 1 h at RT. After that, the membrane was washed six times with 10 mM Tris–HCl, pH 8.0 and the signal corresponding to the activity of HRP was detected using the Pierce ECL Plus Western Blotting Substrate (Thermo Scientific, #32134) (51).

RESULTS

A rapid workflow to visualize circular and linearized mitochondrial genomes with short and expanded D-loops

To visualize human mitochondrial DNA replication using transmission electron microscopy (TEM), asynchronously growing human U-2 OS cancer cells were subjected to the workflow described in detail in the Materials and Methods section. The same workflow with similar results was applied to additional human cancer cell types (HeLa cells) and normal human fibroblasts (BJ cells).

Briefly, U-2 OS cells were subjected to a high-density *in vivo* psoralen-mediated inter-strand DNA cross-linking, and the total DNA (containing both genomic and highly enriched mitochondrial DNA) was extracted using a rapid method (see Materials and Methods). Purified DNA was subjected to partial restriction enzyme digestion with PvuII that cuts only one time in the human mitochondrial DNA (Figure 1). The digested DNA was subjected to a quick procedure to enrich DNA replication intermedietes containing ssDNA (see Materials and Methods) (46,47), followed by BAC-mediated DNA spreading (44). Next, DNA was absorbed on a thin layer of carbon deposited on an electron microscopy grid, positively stained with uranyl acetate, and exposed to low-angle rotary shadowing with platinum, followed by TEM analysis (44,52).

Using TEM, we identified circular dsDNA molecules with an average size of 6.3 microns (corresponding to an average dimension of 17 495 bp) in this experimental condition (Figure 2A). Considering that circular DNA molecules adsorbed on the carbon surface become extended of about 5% of their length (52), we concluded that we are able to visualize and analyze dsDNA circles with an average dimension very close to 16,6 kb, which are *bona fide* human mitochondrial genomes.

As predicted from the early studies (6,8,29) and by the SDM and the RITOLS models of mitochondrial DNA replication (Figure 1A, B), we found that 50% of circular DNA molecules in our samples carried a short D-loop (6,7) with an average size of around 700 nt. This size is very close (assuming 5% stretching in length) to the dimension of 645 nt previously reported for the short D-loop of the mammalian mitochondrial DNA (Figure 2A) (29). The other 50% of the circular DNA molecules analyzed corresponded to non-replicating mitochondrial genomes. Notably, the specific spreading procedure applied in this work clearly allowed for the distinction between ssDNA and dsDNA, thus facilitating the analysis and the recognition of the three-stranded D-loop structure (Figure 2).

We noticed that many circular mitochondrial genomes carrying the short D-loop structure were highly supercoiled when they got adsorbed on the carbon surface. In contrast, the non-replicating circular mitochondrial genomes (lacking D-loop) showed a more relaxed state (Figure 2A). The supercoiled condition of many circular mitochondrial genomes precluded the precise measurements of the length of the short D-loops because their ssDNA stretches became entangled in the supercoiled circular molecules (Figure 2A). However, since the mitochondrial DNA in our samples was exposed to partial digestion with the PvuII enzyme, we could precisely map the D-loop position on mitochondrial DNA molecules that were digested by the restriction enzyme (Figure 2B), taking advantage of the release of the supercoiled state due to the linearization of the mitochondrial genome with PvuII.

Linearized mitochondrial genomes carrying a short D-loop had an average size very close to the circular molecules (17 844 bp) (Figure 2B). We defined segment #1 (from the PvuII site closer to the D-loop to the beginning of the D-loop) that had an average size of 2624 bp (Figure 2B, C) and segment #2 (from the end of the D-loop to the PvuII site more further away from the D-loop) that had an average length of 13396 bp (Figure 2B–D). The average size of the short D-loop on the PvuII linearized mitochondrial genomes was around 700 bp (Figure 2E), very close to the average length of the short D-loops measured on non-digested, circular mitochondrial genomes (Figure 2A). These measurements support the conclusion that linearized DNA molecules carrying short D-loops originated from the PvuII-mediated linearization of the circular mitochondrial genomes (Figure 2A, B, E). From these length measurements we concluded that the short D-loop is always in the same position with respect to the PvuII site closer to the D-loop on all the linearized mitochondrial DNA molecules analyzed.

Next, we set out to confirm that linearized molecules carrying short D-loop originate from the circular mitochondrial genomes digested using PvuII. Purified DNA was divided into two samples. While one sample was exposed to the partial digestion using the restriction enzyme PvuII, the second sample was in parallel treated with BglII, an enzyme that, compared to PvuII, does not have a cut site in the human mitochondrial DNA. Importantly, even after a prolonged search at the electron microscope, the linearized forms of the mitochondrial genomes with short D-loop were not detectable in the sample treated with BglII. Simultaneously, the chromosomal DNA fibers that were co-purified together with the mitochondrial DNA during DNA extraction were properly digested with BglII (as judged by the reduction of their size). Based on this experiment, we concluded that linearized molecules carrying a short D-loop originate from the circular mitochondrial genomes digested using PvuII. Although double-stranded theta structures of mitochondrial DNA (replicating) from cultured cells that are modified by RNase H have been previously reported (20), in all the experiments conducted in this study using three different cell lines (see the next paragraphs), the circular or linearized human mitochondrial genomes carrying classic DNA replication bubbles (theta intermediates) were not found.

During the analysis of the length of PvuII linearized mitochondrial genomes, we realized that while segment #1 had almost always the same length over the molecules analyzed, there were linearized mitochondrial genomes in which the length of the D-loop exceeded the average length of the short D-loop (700 bp). In those molecules with extended D-loops, the length of segment #2 was shorter than the average length (13396 bp) of segment #2 on molecules with the short D-loop, and segment #1 always had the same length in all the molecules analyzed (Figure 2E, D), indicating a process of unidirectional D-loop expansion. We decided to analyze those linearized molecules with short and extended D-loops in more detail.

Unidirectional HS mitochondrial DNA synthesis progression can be clearly analyzed on PvuII linearized human mitochondrial DNA molecules using DNA replication maps

The Strand Displacement Model (SDM) of mitochondrial DNA replication predicts that the progression of the heavy strand (HS) DNA synthesis (leading strand DNA synthesis) displaces the parental heavy strand (strand displacement) (Figure 1A), leading to a unidirectional expansion of the

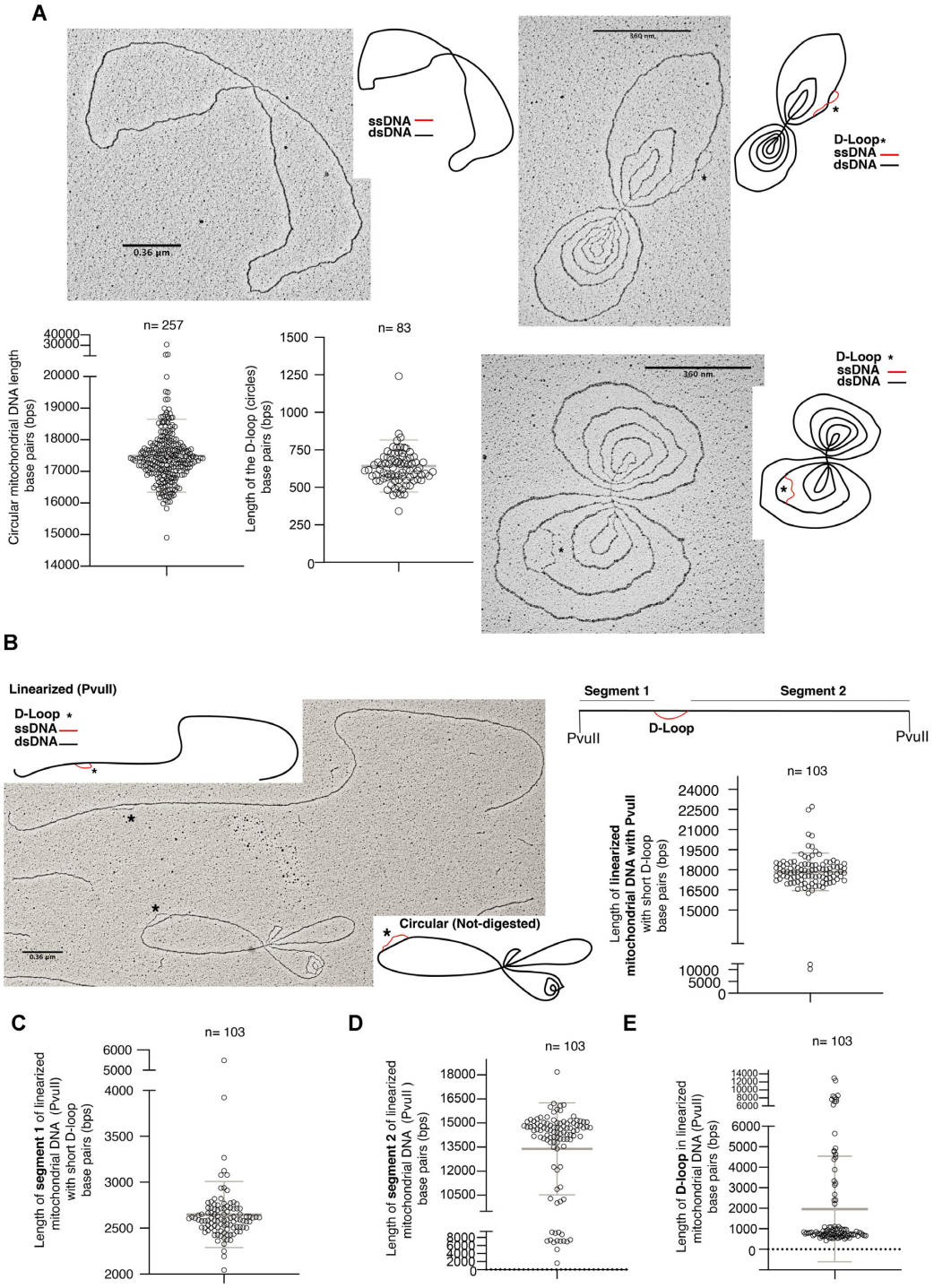

Figure 2. Circular and PvuII-linearized human mitochondrial genomes can be isolated and analyzed using the presented workflow. (**A**) Representative electron microscopy (EM) pictures of circular mitochondrial genomes (without and with short D-loops) with schematic representations indicating dsDNA in black, ssDNA in red, and the position of the short D-loop with an asterisk. Scale bars of 360 nm (in black) corresponding to 1 kilobase pair are reported on each EM picture. Graphs reporting the distribution of the total lengths of the circular mitochondrial genomes and the lengths of the short D-loops are shown. The average length and standard deviation bars are shown on each distribution graph. Data were collected from four independent experiments (U-2 OS cells). The total number of molecules analyzed is $n = 257$ (circles) and $n = 83$ (D-loops). The average length of the dsDNA circles is 17 495 bp (6.3 μm). (**B**) Representative electron microscopy (EM) picture (with schematic representations) of a PvuII-linearized mitochondrial genome next to the circular mitochondrial genome (both structures carrying a short D-loop) with a graph showing the distribution of the total lengths of the PvuII-linearized mitochondrial genomes analyzed with average length and standard deviation bars. The average length of the PvuII-linearized mitochondrial genomes is 17844 bps. A scale bar of 360 nm (1 kbp) (in black) is shown on the EM picture. (**C–E**) Graphs showing the distribution of the lengths of segment #1 (average length 2624 bp), segment #2 (average length 13396 bps), and D-loop (average length 700 bp) measured on the PvuII-linearized mitochondrial DNA molecules analyzed in (B) with average length and standard deviation bars (see the text of the manuscript). Data shown in B–E are from four independent experiments (U-2 OS cells). Total numbers (n) of molecules analyzed are reported on each graph.

short D-loop. Therefore, we decided to build a replication map in which we aligned multiple schematics in scale representations of all linearised mitochondrial genomes analyzed with reported positions, and dimensions, of segment #1, D-loop, and segment #2 (Figure 3A, B).

Linearization of the mitochondrial DNA molecules with the restriction enzyme PvuII allowed a more precise measurement and inspection of the structural features of both short and extended D-loops (Figures 2B and 3A), which were not entangled into the supercoiled circular molecules and were accurately mapped toward the position of the PvuII site (Figure 3A, B).

From the mitochondrial DNA replication map, we concluded that: (i) the short D-loop is always located in the same position with respect to the PvuII cut sites in all the linearized mitochondrial DNA molecules analyzed, except for a few sporadic cases in which segment #1 was longer or shorter and short D-loop was in an unusual position (those sporadic D-loops in unusual position could represent additional initiation sites of the human mitochondrial DNA replication); (ii) in the linearized genomes in which the D-loop was expanded, it expanded only from one side (side of the D-loop further away from the PvuII cut site) as predicted by the SDM and the asynchronous and unidirectional progression of the HS DNA synthesis (Figure 1A and Figure 3A, B); (iii) the D-loop position toward the PvuII cut site fits with previously reported evidence of the D-loop location in the human mitochondrial genome (29). When the estimated positions of the D-loops analyzed in this study were compared to the position of known elements of the human mitochondrial genome like heavy strand promoter (HSP), light strand promoter (LSP), conserved boxes 1–2–3 (CSB 1–2–3), HO, termination associated sequences (TAS) and LO it emerged that the large majority of D-loops identified in this study are localized, as expected from previously reported evidence, between the CSB 1–2–3 and the TAS sequences. (Figure 3B and Supplementary Figures S1A, S4B).

In agreement with previous reports (8), we found that HS mitochondrial DNA replication can displace up to two-thirds of the parental HS. Indeed, we found linearized mitochondrial DNA molecules carrying three strands D-loop structures with ssDNA stretches up to 8000–10 000 nucleotides (Figure 3A). Moreover, out of the 100 linearized mitochondrial DNA genomes carrying the D-loop structure, 75 of them showed a short D-loop with an average length of 700 nt. In contrast, 25 molecules had an expanded D-loop (Figure 3B) in agreement with previous reports on the temporal separation, asynchronous, opposite, and unidirectional progression of HS and LS human mitochondrial DNA replication (10) and with the *in vivo* occupancy of mtSSB protein during human mitochondrial DNA replication (26,32).

Next, we performed the identical structural analysis of the same DNA samples which we analyzed in Figure 3; however, we omitted BND-cellulose/G20 enrichment steps. In those non-enriched samples, we observed the same DNA structures (Supplementary Figure S1A) as in samples that underwent BND-cellulose/G20 enrichment procedure (Figure 3B). We also obtained the same quantitative ratio of mitochondrial DNA replication intermediates when comparing non-enriched and enriched samples (Supplementary Figure S1B). In particular, in both samples, we observed 75% of mitochondrial DNA replication intermediates with short D-loops and 25% intermediates with extended D-loops (Supplementary Figure S1B). Hence, we concluded that enrichment steps do not impact the DNA structures and quantitative ratio obtained in the structural analysis of mitochondrial DNA replication intermediates.

It is of note that even after an extensive search at the electron microscope, we did not observe any classic DNA replication bubble (or theta DNA molecules) in non-enriched nor BND-cellulose/G20 column-enriched samples (Supplementary Figure S1B). Since specific modes of mitochondrial DNA replication entail DNA structures carrying DNA:RNA hybrids (Figure 1), we decided to utilize the dot-blot analysis using the S9.6 antibody recognizing DNA:RNA hybrids. This method is widely used to measure the content of DNA:RNA hybrids in the DNA samples (51). We performed the dot-blot analysis of samples before and after the BND-cellulose/G20 columns-based enrichment procedures. We observed that non-enriched DNA samples contain DNA:RNA hybrids and that the DNA structures carrying DNA:RNA hybrids are very efficiently enriched by the enrichment procedures adopted in this study (Supplementary Figure S1C, D). Moreover, the S9.6 signal we detect in the dot-blot analysis is not due to dsRNA species, but it is specific for DNA:RNA hybrids (Supplementary Figure S1E) (51).

It has been demonstrated that heavily transcribed regions of the ribosomal DNA (rDNA) can be heavily cross-linked *in vivo* by psoralen under experimental conditions identical to the ones utilized in the present study (53). Those regions containing DNA:RNA hybrids can be visualized through the spreading in native and denaturing conditions, low-angle rotary shadowing, and transmission electron microscopy using experimental conditions identical to those utilized in the present study (53).

In supplementary Figures S2 and S3, we report additional examples (with enlarged views) of extended and short D-loops generated during human mitochondrial HS DNA replication.

LS mitochondrial DNA replication intermediates (gapped circles) are clearly distinguishable with the applied spreading and low-angle rotary shadowing conditions

According to the uncoupled and asynchronous model of mitochondrial DNA replication, once the replication of the HS is completed, a fully replicated circular mitochondrial DNA molecule is released (composed of one parental LS and one newly synthesized HS). Simultaneously, the gapped circular mitochondrial genome composed of a full parental HS and an incompletely newly synthesized LS (Figure 1A) is produced. Although these molecules were less frequent than the HS mitochondrial DNA replication intermediates carrying short or extended D-loops, we were able to identify circular and incompletely replicated gapped human mitochondrial genomes of an average length of 17 500 bp (Figure 4). This dimension is very close to non-replicating circular human mitochondrial genomes (Figures 2A and 4).

In some of these gapped circular mitochondrial genomes, it was possible to identify single-strand DNA gaps of

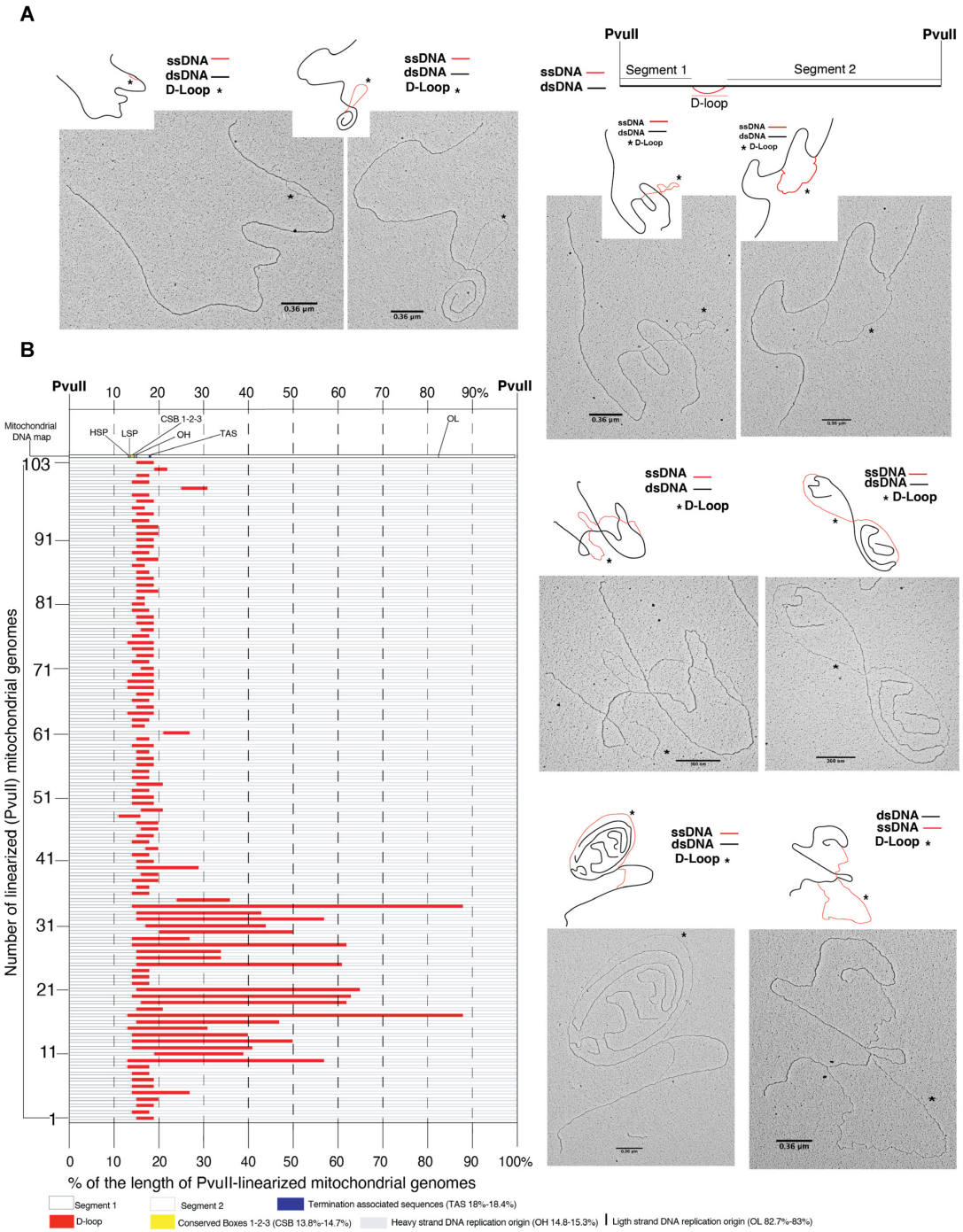

Figure 3. Unidirectional expansion of the human mitochondrial D-loop during HS DNA replication can be analyzed using replication maps built on PvuII-linearized mitochondrial genomes. (**A**) Representative EM pictures of HS mitochondrial DNA replication intermediates (PvuII-linearized mitochondrial genomes) with schematic representations of the position of dsDNA (black), ssDNA (red), and the position of the D-loop (asterisks). A schematic representation of the PvuII-linearized mitochondrial genome with the indicated positions of segment #1 (black), segment #2 (black), and the D-loop (black, red) are shown. A scale bar of 360 nm (1 kbp) (in black) is shown on each EM picture. (**B**) Replication map with schematized representations of 103 aligned PvuII-linearized mitochondrial genomes with the indicated positions of segment #1 (dark gray), D-loop (red), and segment #2 (light gray). The length of the molecules is expressed as a percentage of the total length so that all the molecules and their structural features can be aligned on the same map. A graphical map of the human mitochondrial genome linearized with PvuII (where the lengths are expressed as percentages of the total length of the mitochondrial genome) is also aligned with the replication map so that the estimated position of short and extended D-loops can be compared to the positions of known human mitochondrial DNA sequences like Heavy Strand Promoter (HSP), Light Strand Promoter (LSP), Conserved Boxes 1–2-3 (CSB 1–2–3, yellow), Heavy Strand Origin of Replication (OH), Light Strand Origin of Replication (OL), Termination Associated Sequences (TAS, blue). For each sequence element, the coordinates utilized to build the graphical map are shown as a percentage of the total length of the PvuII-linearized mitochondrial genome. The numbers of PvuII-linearized genomes analyzed and numbers of mitochondrial genomes with short and expanded D-loops (see the text) are shown. The 25 molecules with the extended D-loops represent the sum total of unambiguous replication intermediates. Source material: U-2 OS cells.

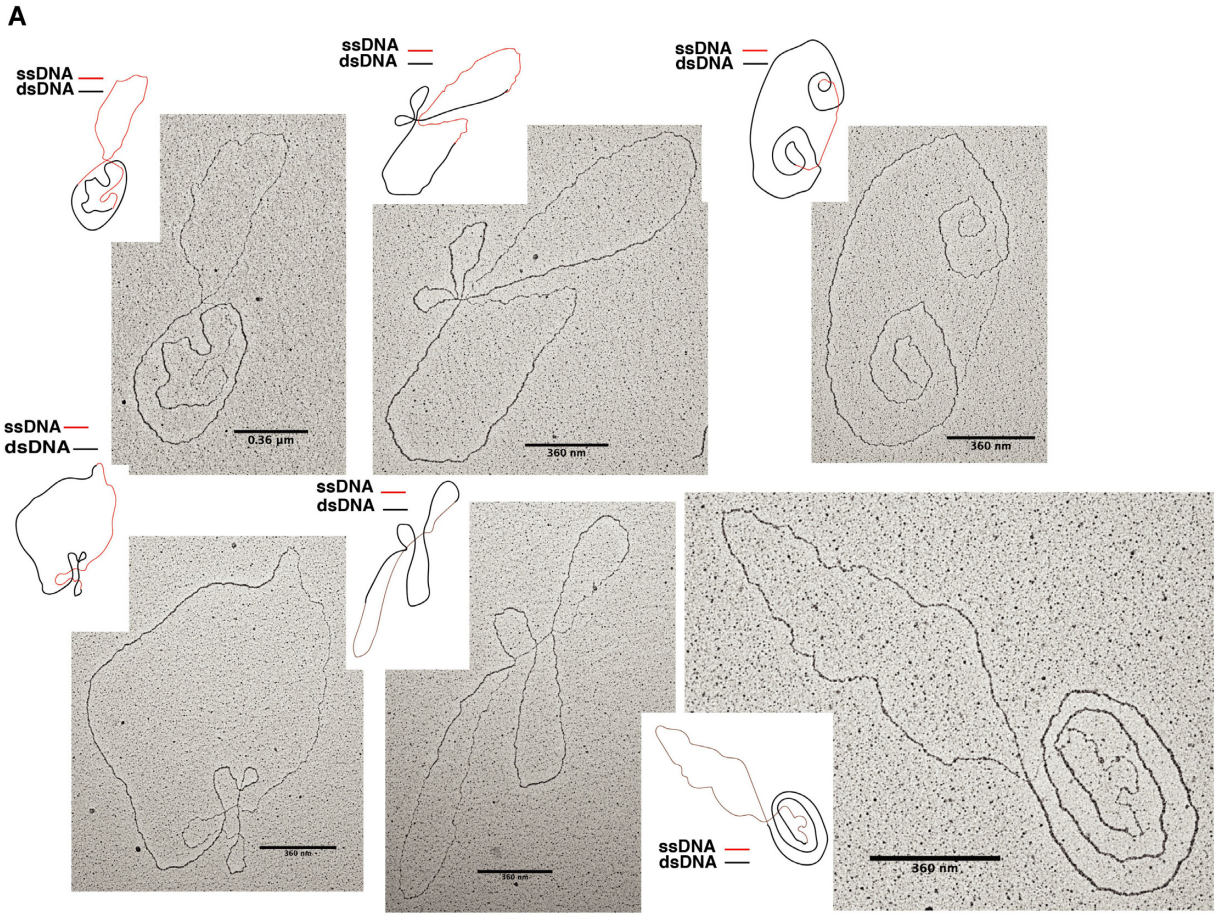

Figure 4. LS mitochondrial DNA replication fork progression can be followed by analyzing the gapped mitochondrial genomes. (**A**) Representative EM pictures of LS mitochondrial DNA replication intermediates (gapped circles) with schematic representations of the position of dsDNA (black) and ssDNA (red). A scale bar of 360 nm corresponding to 1 kbp is shown on each EM picture. Source material: U-2 OS cells.

around 10 000 nucleotides (Figure 4). This suggests that HS DNA replication can be completed (and one fully replicated mitochondrial genome released) when approximately two-thirds of the LS DNA synthesis is missing on the second replicating mitochondrial DNA strand (Figure 4 and Figure 1A). This observation supports the asynchronous, uncoupled, and opposite progression of HS and LS DNA replication during mammalian mitochondrial DNA replication as proposed in early studies (3,4,8,10).

High density *in vivo* psoralen-mediated DNA inter-strand cross-linking coupled to denaturing spreading allow the inspection of the chromatin structure of human mitochondrial DNA and the analysis of the *in vivo* three-strand DNA architecture of the human mitochondrial D-loop

High-density *in vivo* psoralen-mediated inter-strand DNA cross-linking coupled with 'native' or 'denaturing' spreading of naked purified DNA, and Transmission Electron Microscopy (TEM) were applied in early studies to visualize viral, episomal, and genomic DNA replication intermediates and to inspect theirs *in vivo* chromatin structure (44–46,48,53,54). According to the standard 'native' spreading protocol (see Materials and Methods), the DNA molecules are analyzed under mild denaturing conditions so that the two complementary ssDNA filaments of the DNA double helix remained paired during the experimental procedure (Figures 2–4). Therefore, the DNA molecules appear as fibers with an average thickness of 10 nm, well distended and separated on the spreading surface (without getting entangled) when they are adsorbed to the carbon surface. That facilitates inspection of their structural features through TEM.

In the variant of the standard 'native' spreading protocol, called 'denaturing spreading', the DNA fibers are handled and subsequently spread in denaturing conditions (see Material and Methods). That leads to the complete dissociation of the complementary ssDNA filaments of a DNA fiber, except for those points on the filaments, where adjacent DNA bases present on the opposite complementary DNA strands of the double helix were covalently cross-linked *in vivo* as a consequence of UVA-mediated psoralen DNA inter-strand cross-linking (45,46,48,53). Tightly bound DNA-protein complexes such as nucleosomes will shield the DNA molecule, preventing the occurrence of inter-strand DNA cross-links, except for the inter-nucleosome linkers, which will experience inter-strand cross-linking. Simultaneously, nucleosome-free regions (or, in general, low occupancy

regions) will experience a higher density of inter-strand DNA cross-links (see Material and Methods). Heavily transcribed genomic regions (containing DNA:RNA hybrids) will also experience high-density DNA inter-strand cross-links compared to genome regions assembled in tight nucleosome arrays (53).

With the 'denaturing' spreading technique, DNA molecules that were assembled in nucleosome arrays *in vivo* will be heavily cross-linked at the inter-nucleosomal spacers (in this experimental condition around 85–90% of linker regions between nucleosomes will be cross-linked). Therefore, with the denaturing spreading, DNA molecules that were assembled in tight nucleosome arrays will appear as DNA fibers composed of arrays of closely spaced ssDNA bubbles of an average length of around 150 nt, and the ssDNA filaments composing those bubbles will have an average thickness distributed around 5 nm. On the contrary, nucleosome-free regions, or DNA regions not tightly and densely bound by proteins (or heavily transcribed regions containing DNA:RNA hybrids) (53), will be heavily cross-linked and will appear as dsDNA fibers with an average thickness of 10 nm. Therefore, under denaturing conditions, the high density of inter-strand cross-links on the DNA fiber will prevent the two ssDNA filaments composing a DNA fiber from dissociating.

To test the efficiency of the denaturing spreading protocol and to measure the density of the DNA inter-strand cross-links on the human mitochondrial DNA replication intermediates analyzed, we subjected our DNA samples to denaturing spreading conditions. As it may be noticed from Figure 5A, we observed a segment of a chromosomal DNA fiber with closely spaced single-strand DNA bubbles of an average length of 150 nt, indicative of *in vivo* assembly of that segment of the chromosomal DNA fiber into a tight nucleosome array. Simultaneously, on the same DNA molecule, we observed an adjacent region where the inter-strand DNA cross-links were more interspersed, suggesting the presence of tightly bound non-nucleosomal DNA-protein complexes with higher occupancy. Alternatively, those regions could represent *in vivo* topological arrangements of the DNA fiber (positive super-coilings) that inhibit psoralen intercalation within the adjacent DNA bases of complementary strands of the DNA fiber preventing subsequent covalent inter-strand DNA cross-linking by psoralen in the presence of UVA irradiation (55).

Next, we decided to use the same denaturing spreading protocol to analyze circular and PvuII-linearized mitochondrial DNA molecules. We found that contrary to chromosomal DNA filaments, both circular and PvuII-linearized mitochondrial genomes showed a high frequency of long and heavily cross-linked DNA stretches (Figure 5A–C). In all mitochondrial DNA molecules analyzed (either circular or linearized genomes), we rarely identified regularly and closely spaced arrays of single-strand DNA bubbles of around 150 nts. This observation indicates that the human mitochondrial genome is not assembled into tight nucleosome arrays in agreement with previous reports on the specific non-nucleosomal chromatin structure of the human mitochondrial genome (56).

To confirm that the PvuII-linearized mitochondrial DNA genomes subjected to denaturing spreading were the same molecules as those analyzed in native conditions, we built a replication map using denatured and linearized mitochondrial genomes. We verified that the same structural features observed in native conditions were preserved: the dimension of segment #1, the position and dimension of the short D-loop, and the dimension of segment #2 (Supplementary Figure S4). Similar to the native spreading analysis, also the 'denaturing' spreading confirmed that the position of the large majority of the short D-loops analyzed in this study is comprised between the CSB 1–2–3 and the TAS sequences (Supplementary Figure S4B).

As an example of the utilization of the denaturing spreading technique to the study of the DNA structure of the human mitochondrial genome, we applied denaturing spreading to analyze the fine chromatin structure of the region carrying the short D-loop on PvuII-linearized mitochondrial DNA molecules (Figure 5D). We found that the D-loop was always composed of three DNA strands in all the analyzed molecules. In particular, it was always possible to identify the single-stranded side of the short D-loops and heavily cross-linked dsDNA stretches (or ssDNA bubbles of heterogeneous dimensions) on the opposite side of the D-loop structure (Figure 5D).

DISCUSSION

We modified and optimized an already well-established protocol for the visualization of chromosomal DNA replication intermediates and adapted it to create a rapid workflow to analyze human mitochondrial DNA replication intermediates (in parallel to the analysis of chromosomal DNA replication intermediates) (46) through low-angle rotary shadowing and TEM.

The technique relies on high density *in vivo* psoralen-mediated inter-strand cross-linking of the DNA fibers (in the conditions described in this study, we create inter-strand cross-links on around 85–90% of the inter-nucleosome spacers on human chromosomal DNA fibers) (46), which gives the advantage of preserving *in vivo* DNA structures by preventing *in vitro* isomerization, branch migration (and other topological transactions on the DNA molecules) that can occur immediately after the deproteinization step and rupture of the topological domains during DNA purification (12,57). The presence of psoralen mono-adducts on the exposed DNA bases on the ssDNA stretches (58) could also prevent *in vitro* reannealing between ssDNA stretches present on several mitochondrial DNA replication intermediates and ssRNA, which may occur after deproteinization during genomic DNA purification (32). On the contrary, *in vivo* DNA structures carrying DNA:RNA hybrids can be heavily cross-linked and preserved along with the subsequent steps of DNA extraction (53). Although all the bubble-like mitochondrial DNA replication intermediates isolated and analyzed in this study (either on circular or on linearized mitochondrial DNA molecules) contain long ssDNA stretches, previous works identified DNA replication bubbles (theta intermediates) carrying RNA tracts on replicating mitochondrial DNA molecules (20). Future studies utilizing tightly controlled conditions of *in vivo* psoralen-mediated DNA inter-strand cross-linking will be required to clarify the *in vivo* quantitative ratio between mitochon-

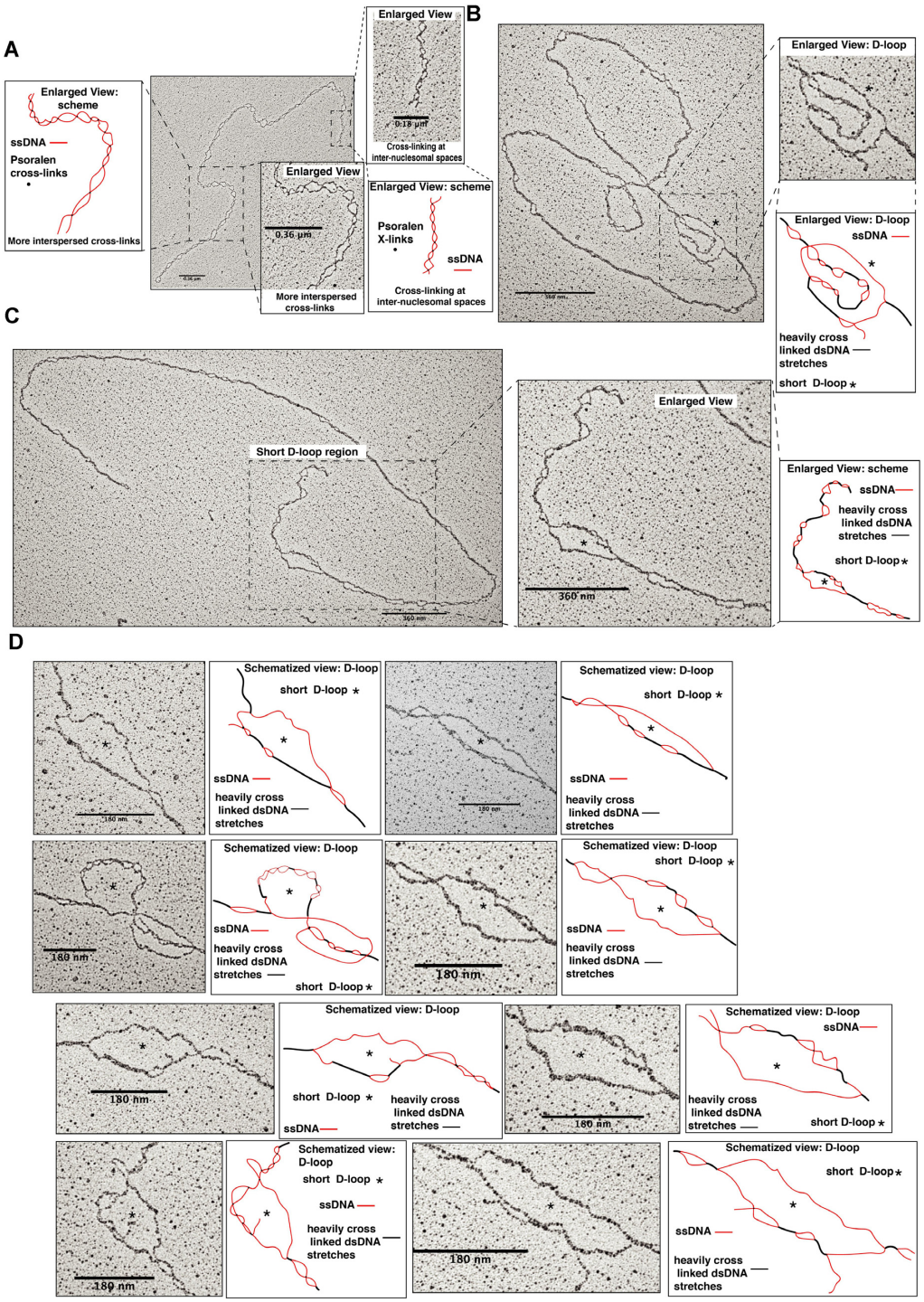

Figure 5. High density *in vivo* psoralen DNA inter-strand cross-linking coupled to denaturing spreading allows to visualize the *in vivo* three-strand DNA structure of the mammalian mitochondrial D-loop. (**A**) Representative EM picture of a chromosomal DNA fiber subjected to denaturing spreading with a schematic representation of the regions of the fiber heavily cross-linked by psoralen in black and ssDNA bubbles due to the absence of DNA inter-strand cross-links in red. Enlarged views of regions of the chromosomal DNA fiber with regularly spatially closed interspaced cross-links (indicative of assembly in a tight nucleosomal array) or with more interspersed cross-links are shown (see the text). Scale bars of 360 nm (1 kbp) or 180 nm (0.5 kbp) (in black) are shown on each EM picture. (**B**, **C**) Representative EM pictures (and enlarged views) of circular (B) or PvuII-linearized (C) mitochondrial genomes subjected to denaturing spreading (see the text). Scale bars of 360 and 180 nm corresponding to 1 kbp and 0.5 kbp, respectively, are reported on each picture. Schematized representations are shown with heavily cross-linked regions in black and ssDNA bubbles due to the absence of DNA inter-strand cross-links in red. The position of the D-loop structure is indicated by the asterisk. (**D**) Enlarged views (EM pictures) and schematized representations of the D-loop region on PvuII-linearized mitochondrial DNA molecules subjected to denaturing spreading (see the text). Heavily cross-linked stretches of dsDNA (and ssDNA denaturation bubbles) are clearly visible in the D-loop structures opposite to the side of the D-loop, which is completely single-stranded, thus demonstrating the *in vivo* three-strands structure of the human mitochondrial D-loop. Scale bars of 180 nm corresponding to 0.5 kbp are reported on each picture. The position of the D-loop structure is indicated by the asterisk. Source material: U-2 OS cells.

drial DNA replication bubbles with long ssDNA stretches and theta replication intermediates carrying RNA tracts. In this context, to better clarify which is the coverage of the mtSSB on the displaced parental heavy strand at the level of single mitochondrial DNA molecules, we envisage a future implementation of the technique presented in this study that combines TEM analysis and protein–DNA cross-linking.

Moreover, it has been proposed that the absence of theta intermediates of mitochondrial DNA replication is due to the experimental-mediated degradation of the RNA component of the RITOLS intermediates (see Figure 1B) (20,59), while in other studies, it has been shown that classical DNA replication bubbles with tracts of RNA can be created by *in vitro* re-annealing reactions between bubble-like mitochondrial DNA replication intermediates carrying long ssDNA stretches and ssRNA present in the samples (32), although fully duplex DNA replication bubbles with the displaced parental heavy strand completely covered by the annealed RNAs were never generated using this *in vitro* procedure. Therefore, additional studies employing tightly controlled conditions of in vivo DNA inter-strand cross-linking will be required to further clarify this issue.

High density *in vivo* psoralen-mediated inter-strand DNA cross-linking also allows the utilization of the 'denaturing' spreading technique to gain additional structural information on the DNA intermediates analyzed. The denaturing spreading technique applied here allows clear visualization of the three-stranded *in vivo* DNA structure of the human mitochondrial D-loop, confirming previously reported evidence obtained in early studies using sedimentation techniques and Transmission Electron Microscopy (TEM) (Figure 5) (6,7).

The optimized and quick DNA extraction procedure utilized here allows the preparation of human genomic DNA samples heavily enriched for mitochondrial DNA without the need of purifying it to homogeneity with time-consuming density gradients-based techniques. This rapid procedure also eliminates the negative consequences of prolonged manipulation of the DNA structures that are unavoidable when sedimentation approaches are utilized to analyze the human mitochondrial DNA.

Genomic DNA samples enriched for the mitochondrial DNA are partially digested with PvuII enzyme, and DNA replication intermediates carrying ssDNA are enriched on anion-exchange (QIAGEN Genomic-tip 20/G) or benzoylated-naphtoylated-diethyl-amino-ethyl-cellulose (BDN-cellulose) columns (see Materials and Methods). Importantly, this enrichment of ssDNA-containing DNA intermediates reduces the microscope time required to find mitochondrial DNA replication intermediates, but it does not influence the quantitative ratios of mitochondrial DNA replication intermediates. Indeed, the same experimental conclusions and quantitative ratios can be obtained working on non-enriched samples (Supplementary Figure S1A, B), although the time for the analysis at the electron microscope will be longer.

It is of note that DNA replication, repair, recombination, and transcription intermediates always contain short stretches of ssDNA due to the inherent asymmetry of the DNA-synthesizing machines involved in those DNA-mediated processes. In particular, incomplete alignment between the newly synthesized strands and incomplete pairing of the ends of the nascent strands with the templates in those DNA-related processes create ssDNA regions that are visible at the electron microscope. Those DNA structures carrying stretches of ssDNA are very efficiently enriched by the BND-cellulose and G20 columns, the two enrichment procedures utilized in this study.

It remains a possibility that fully duplex theta structures carrying long RNA tracts that cover the entire displaced parental HS (generated during the human mitochondrial DNA replication) could potentially escape the capturing by the BND-cellulose and G20 columns based enrichment procedures. To exclude this possibility, it is advisable to perform analysis comparing enriched and non-enriched samples in parallel, as done in this study (Figure 3 and Supplementary Figure S1A, B).

Thanks to the partial digestion of the mitochondrial genomes with PvuII, it is possible to analyze, in parallel, circular, and linearized mitochondrial DNA genomes with the advantage that the structural features of the HS DNA replication can be inspected in more detail (due to the absence of supercoiling). Moreover, the unidirectional progression of HS replication (D-loop expansion) can be mapped towards the PvuII restriction sites and can be followed using DNA replication maps aligning multiple schematized representations of PvuII linearized mitochondrial DNA genomes (9) (Figures 2 and 3).

The use of the replication maps as described in this study (multiple graphical alignments of schematized mitochondrial genomes linearized with PvuII) allows the identification of short sporadic D-loops located outside the average position of most of the short D-loops (Figure 3B and Supplementary Figure S1A, S4B). Therefore, the replication maps presented in this study might represent a valuable tool for identifying additional putative mitochondrial DNA replication initiation sites utilized with very low frequency. Importantly, the mapping of the location of the short D-loops toward known markers present in the human mitochondrial genome highlighted that most short D-loop structures visualized in this study localized between the CSB 1–2–3 and TAS sequences according to previously reported evidence (29). Hence, this study demonstrated that the method presented here allows executing a precise analysis of the location of the structural features of the human mitochondrial DNA replication (Figure 2–5 and Supplementary Figures S1 and S4).

Moreover, the measurements done by electron microscopy in this specific experimental condition have a 5–10% tolerance range, therefore the estimated position of the D-loop structures analyzed in this study compared to the position of known mammalian mitochondrial DNA sequences could be influenced by this unavoidable level of uncertainty. Importantly, all the results obtained on linearized mitochondrial genomes can be confirmed on the circular genomes. However, the high level of supercoiling frequently prevents a detailed structural inspection because of the entangling of the long single-strand DNA stretches into the supercoiled dsDNA circles.

LS DNA synthesis can also be followed on gapped circular DNA molecules that are more relaxed (Figure 4) due

to the discontinuity present on the double helix. The BAC spreading procedure of naked and highly purified DNA samples coupled to positive staining and optimized low-angle rotary shadowing (electron beam evaporation) allows the clear distinction of dsDNA from ssDNA based on the different thicknesses of the DNA fiber in this experimental condition. The use of this specific spreading technique is particularly advantageous considering that several human mitochondrial DNA replication intermediates carry long stretches of ssDNA. Thanks to the clear visualization of ssDNA, it is possible to identify extended D-loops (HS replication) and gapped circles (LS replication) with ssDNA stretches up to 8–10 thousand nucleotides (Figure 3 and 4), strongly supporting the asynchronous, uncoupled, opposite, and unidirectional mode of mammalian mitochondrial DNA replication in agreement with early pulse labeling experiments (10) and electron microscopy observations (8). Importantly, all the stretches of ssDNA on the HS and LS replication intermediates analyzed did not show internal dsDNA regions indicating that in the vast majority of the events under this experimental condition, DNA replication initiation is restricted to OH and OL according to early studies (4).

Although RNase A is utilized to eliminate the large amount of free single-strand RNA (ssRNA) and double-strand RNA (dsRNA) present in the DNA preparations (to avoid technical problems in several steps of the protocol and unscheduled formation of DNA intermediates *in vitro* during cell lysis and deproteinization) (see Materials and Methods) (32), the same DNA structures can be identified if RNase A is omitted from the protocol and the DNA samples are prepared, enriched and analyzed without getting into contact with any RNase activity that can degrade ssRNA, dsRNA or DNA/RNA hybrids.

Although the RNase-free protocol is feasible, the massive amount of fragmented ssRNA fibers will make the EM analysis tedious, and it will decrease the efficiency of the enrichment process and the quality of the EM visualization data. Notably, the high density *in vivo* inter-strand DNA cross-linking technique utilized in this study would also stabilize and preserve DNA:RNA hybrids even in the presence of RNase A treatment during the DNA extraction (53,60) (Supplementary Figure S1C-D-E).

With this workflow, we were able to confirm previously reported conclusions about the uncoupled and asynchronous progression of the human mitochondrial DNA replication (8,61). The experimental evidence reported here support a spatial and temporal separation between HS and LS DNA synthesis and the unidirectional and opposite progression of HS and LS DNA synthesis, which are essential requirements for the uncoupled mode of the human mitochondrial DNA replication as postulated by the SDM and RITOLS (Figures 1, 3 and 4).

As discussed above, we did not observe theta intermediates using the protocol described in this study. However, additional studies, e.g., applying the technique on a different starting material such as solid tissues, are needed to shed additional light on the mechanisms of mitochondrial DNA replication.

Finally, with the applied workflow, the analysis of chromosomal DNA replication intermediates can be conducted as previously described (46) in parallel with the analysis of LS and HS human mitochondrial DNA replication. We would like to underline that the technique described in this study is specifically suitable to study mitochondrial DNA replication intermediates purified from human cultured cells. In the present study, we isolated the same human mitochondrial DNA replication intermediates from cancer cells (U-2 OS, HeLa) or primary cells (BJ) (Supplementary Figure S5). In future studies, it will be beneficial to apply this methodology to cells that grow in suspension. Previous transmission electron microscopy analysis of mitochondrial DNA replication intermediates demonstrated that the extent of preservation of RNA tracts in the mammalian mitochondrial DNA replication intermediates is methodology-dependent (20). In organello DNA and RNA labeling on isolated mitochondria from solid tissues followed by psoralen-mediated DNA inter-strand cross-linking indicated that RITOLS might be a physiological mechanism of mitochondrial DNA replication in solid tissues (21,59). Currently, the method presented in this study relies on the high density in vivo psoralen-mediated DNA inter-strand cross-linking and was tested to analyze mtDNA replication intermediates from cultured human cells. However, it would be beneficial to adapt further and optimize the technique to obtain a high-density of *in vivo* psoralen-mediated DNA inter-strand cross-linking of the mitochondrial DNA inside the entire cells when the entire cells are still embedded in the solid tissue. This would provide new insights into the mechanism of the human mitochondrial DNA replication, especially for the RITOLS mode of replication that appears to be more frequent in the mitochondrial DNA replication intermediates extracted from solid tissues (20,21,59).

Although future implementations of electron microscopy techniques like *in situ* mapping of the newly synthesized strands will be required to provide further insights into the mechanism of mitochondrial DNA replication and transcription, the workflow presented here represents a rapid method to investigate heavy and light strands mitochondrial DNA replication with unprecedented clarity.

DATA AVAILABILITY

All the data generated in this study are available upon request to the corresponding authors.

SUPPLEMENTARY DATA

Supplementary Data are available at NAR Online.

ACKNOWLEDGEMENTS

We thank Dana Branzei for the critical reading of the manuscript and suggestions and Ylli Doksani for providing the optimized protocol of genomic DNA extraction heavily enriched for the mitochondrial DNA. We thank the IFOM electron microscopy Technological Development Unit (TDU DNA/single molecules).

Author contributions: M.K., M.F., D.P. and M.G. designed the experiments. M.K. performed the experiments. D.P. and M.G. prepared EM samples and acquired EM pictures.

M.G. analyzed the EM data and wrote the manuscript. M.F. and M.G. supervised the study. M.F. provided financial support. All authors read and approved the manuscript.

FUNDING

Fondazione AIRC per la Ricerca sul Cancro (to M.F.); M.K. has received funding from the European Union's Horizon 2020 research and innovation program under the Marie Sklodowska-Curie grant agreement No 707600, and from the Fondazione Umberto Veronesi (Milano, Italy), Post-doctoral Fellowships 2019 and 2020. Funding for open access charge: European Union's Horizon 2020 research and innovation program under the Marie Sklodowska-Curie grant agreement No 707600; Fondazione Umberto Veronesi (Milano, Italy), Post-doctoral Fellowships 2019 and 2020; Fondazione AIRC per la Ricerca sul Cancro.
Conflict of interest statement. None declared.

REFERENCES

1. Anderson,S., Bankier,A.T., Barrell,B.G., de Bruijn,M.H., Coulson,A.R., Drouin,J., Eperon,I.C., Nierlich,D.P., Roe,B.A., Sanger,F. *et al.* (1981) Sequence and organization of the human mitochondrial genome. *Nature*, **290**, 457–465.
2. Crews,S., Ojala,D., Posakony,J., Nishiguchi,J. and Attardi,G. (1979) Nucleotide sequence of a region of human mitochondrial DNA containing the precisely identified origin of replication. *Nature*, **277**, 192–198.
3. Martens,P.A. and Clayton,D.A. (1979) Mechanism of mitochondrial DNA replication in mouse L-cells: localization and sequence of the light-strand origin of replication. *J. Mol. Biol.*, **135**, 327–351.
4. Tapper,D.P. and Clayton,D.A. (1981) Mechanism of replication of human mitochondrial DNA. Localization of the 5' ends of nascent daughter strands. *J. Biol. Chem.*, **256**, 5109–5115.
5. Margolin,K., Doda,J.N. and Clayton,D.A. (1981) Mechanism of mitochondrial DNA replication in mouse L cells: localization of alkali-sensitive sites at the two origins of replication. *Plasmid*, **6**, 332–341.
6. Kasamatsu,H., Robberson,D.L. and Vinograd,J. (1971) A novel closed-circular mitochondrial DNA with properties of a replicating intermediate. *Proc. Natl. Acad. Sci. U.S.A.*, **68**, 2252–2257.
7. Arnberg,A., van Bruggen,E.F. and Borst,P. (1971) The presence of DNA molecules with a displacement loop in standard mitochondrial DNA preparations. *Biochim. Biophys. Acta*, **246**, 353–357.
8. Robberson,D.L., Kasamatsu,H. and Vinograd,J. (1972) Replication of mitochondrial DNA. Circular replicative intermediates in mouse L cells. *Proc. Natl. Acad. Sci. U.S.A.*, **69**, 737–741.
9. Kasamatsu,H. and Vinograd,J. (1973) Unidirectionality of replication in mouse mitochondrial DNA. *Nat. New Biol.*, **241**, 103–105.
10. Berk,A.J. and Clayton,D.A. (1974) Mechanism of mitochondrial DNA replication in mouse L-cells: asynchronous replication of strands, segregation of circular daughter molecules, aspects of topology and turnover of an initiation sequence. *J. Mol. Biol.*, **86**, 801–824.
11. Nass,M.M. (1980) Pulse-label analysis and mapping of the two terminal regions of asynchronous complementary strand replication of mitochondrial DNA in transformed hamster cells. *J. Mol. Biol.*, **140**, 257–281.
12. Bogenhagen,D.F. and Clayton,D.A. (2003) The mitochondrial DNA replication bubble has not burst. *Trends Biochem. Sci.*, **28**, 357–360.
13. Brown,T.A., Cecconi,C., Tkachuk,A.N., Bustamante,C. and Clayton,D.A. (2005) Replication of mitochondrial DNA occurs by strand displacement with alternative light-strand origins, not via a strand-coupled mechanism. *Genes Dev.*, **19**, 2466–2476.
14. Clayton,D.A. and Vinograd,J. (1967) Circular dimer and catenate forms of mitochondrial DNA in human leukaemic leucocytes. *Nature*, **216**, 652–657.
15. Holt,I.J., Lorimer,H.E. and Jacobs,H.T. (2000) Coupled leading- and lagging-strand synthesis of mammalian mitochondrial DNA. *Cell*, **100**, 515–524.
16. Yang,M.Y., Bowmaker,M., Reyes,A., Vergani,L., Angeli,P., Gringeri,E., Jacobs,H.T. and Holt,I.J. (2002) Biased incorporation of ribonucleotides on the mitochondrial L-strand accounts for apparent strand-asymmetric DNA replication. *Cell*, **111**, 495–505.
17. Holt,I.J. and Jacobs,H.T. (2003) Response: the mitochondrial DNA replication bubble has not burst. *Trends Biochem. Sci.*, **28**, 355–356.
18. Yasukawa,T., Yang,M.Y., Jacobs,H.T. and Holt,I.J. (2005) A bidirectional origin of replication maps to the major noncoding region of human mitochondrial DNA. *Mol. Cell*, **18**, 651–662.
19. Yasukawa,T., Reyes,A., Cluett,T.J., Yang,M.Y., Bowmaker,M., Jacobs,H.T. and Holt,I.J. (2006) Replication of vertebrate mitochondrial DNA entails transient ribonucleotide incorporation throughout the lagging strand. *EMBO J.*, **25**, 5358–5371.
20. Pohjoismaki,J.L., Holmes,J.B., Wood,S.R., Yang,M.Y., Yasukawa,T., Reyes,A., Bailey,L.J., Cluett,T.J., Goffart,S., Willcox,S. *et al.* (2010) Mammalian mitochondrial DNA replication intermediates are essentially duplex but contain extensive tracts of RNA/DNA hybrid. *J. Mol. Biol.*, **397**, 1144–1155.
21. Reyes,A., Kazak,L., Wood,S.R., Yasukawa,T., Jacobs,H.T. and Holt,I.J. (2013) Mitochondrial DNA replication proceeds via a 'bootlace' mechanism involving the incorporation of processed transcripts. *Nucleic Acids Res.*, **41**, 5837–5850.
22. Cluett,T.J., Akman,G., Reyes,A., Kazak,L., Mitchell,A., Wood,S.R., Spinazzola,A., Spelbrink,J.N. and Holt,I.J. (2018) Transcript availability dictates the balance between strand-asynchronous and strand-coupled mitochondrial DNA replication. *Nucleic Acids Res.*, **46**, 10771–10781.
23. Bowmaker,M., Yang,M.Y., Yasukawa,T., Reyes,A., Jacobs,H.T., Huberman,J.A. and Holt,I.J. (2003) Mammalian mitochondrial DNA replicates bidirectionally from an initiation zone. *J. Biol. Chem.*, **278**, 50961–50969.
24. Ciesielski,G.L., Oliveira,M.T. and Kaguni,L.S. (2016) Animal mitochondrial DNA replication. *Enzymes*, **39**, 255–292.
25. Holt,I.J. and Jacobs,H.T. (2014) Unique features of DNA replication in mitochondria: a functional and evolutionary perspective. *Bioessays*, **36**, 1024–1031.
26. Falkenberg,M. (2018) Mitochondrial DNA replication in mammalian cells: overview of the pathway. *Essays Biochem.*, **62**, 287–296.
27. Wanrooij,S. and Falkenberg,M. (2010) The human mitochondrial replication fork in health and disease. *Biochim. Biophys. Acta*, **1797**, 1378–1388.
28. Zinovkina,L.A. (2019) DNA replication in human mitochondria. *Biochemistry (Mosc)*, **84**, 884–895.
29. Nicholls,T.J. and Minczuk,M. (2014) In D-loop: 40 years of mitochondrial 7S DNA. *Exp. Gerontol.*, **56**, 175–181.
30. Jemt,E., Persson,O., Shi,Y., Mehmedovic,M., Uhler,J.P., Davila Lopez,M., Freyer,C., Gustafsson,C.M., Samuelsson,T. and Falkenberg,M. (2015) Regulation of DNA replication at the end of the mitochondrial D-loop involves the helicase TWINKLE and a conserved sequence element. *Nucleic. Acids. Res.*, **43**, 9262–9275.
31. Pohjoismaki,J.L., Wanrooij,S., Hyvarinen,A.K., Goffart,S., Holt,I.J., Spelbrink,J.N. and Jacobs,H.T. (2006) Alterations to the expression level of mitochondrial transcription factor A, TFAM, modify the mode of mitochondrial DNA replication in cultured human cells. *Nucleic. Acids. Res.*, **34**, 5815–5828.
32. Miralles Fuste,J., Shi,Y., Wanrooij,S., Zhu,X., Jemt,E., Persson,O., Sabouri,N., Gustafsson,C.M. and Falkenberg,M. (2014) In vivo occupancy of mitochondrial single-stranded DNA binding protein supports the strand displacement mode of DNA replication. *PLos Genet.*, **10**, e1004832.
33. Kaur,P., Longley,M.J., Pan,H., Wang,H. and Copeland,W.C. (2018) Single-molecule DREEM imaging reveals DNA wrapping around human mitochondrial single-stranded DNA binding protein. *Nucleic Acids Res.*, **46**, 11287–11302.
34. Fuste,J.M., Wanrooij,S., Jemt,E., Granycome,C.E., Cluett,T.J., Shi,Y., Atanassova,N., Holt,I.J., Gustafsson,C.M. and Falkenberg,M. (2010) Mitochondrial RNA polymerase is needed for activation of the origin of light-strand DNA replication. *Mol. Cell*, **37**, 67–78.
35. Brennicke,A. and Clayton,D.A. (1981) Nucleotide assignment of alkali-sensitive sites in mouse mitochondrial DNA. *J. Biol. Chem.*, **256**, 10613–10617.

36. Clayton,D.A. (1982) Replication of animal mitochondrial DNA. *Cell*, **28**, 693–705.
37. Kleinschmidt,A.K., Burton,A. and Sinsheimer,R.L. (1963) Electron microscopy of the replicative form of the DNA of the bacteriophage Phi-X174. *Science*, **142**, 961.
38. Kleinschmidt,A.K. (1968) Monolayer techniques in electron microscopy of nucleic acid molecules. *Methods Enzymol.*, **12**, 361.
39. Williams,R.C. and Wyckoff,R.W. (1945) Electron shadow micrography of the tobacco mosaic virus protein. *Science*, **101**, 594–596.
40. Clayton,D.A. and Shadel,G.S. (2014) Purification of mitochondria by sucrose step density gradient centrifugation. *Cold Spring Harb. Protoc.*, **2014**, pdb prot080028.
41. Clayton,D.A. and Shadel,G.S. (2014) Isolation of mitochondria from cells and tissues. *Cold Spring Harb. Protoc.*, **2014**, pdb top074542.
42. Reyes,A., Yasukawa,T., Cluett,T.J. and Holt,I.J. (2009) Analysis of mitochondrial DNA by two-dimensional agarose gel electrophoresis. *Methods Mol. Biol.*, **554**, 15–35.
43. Reyes,A., Yasukawa,T. and Holt,I.J. (2007) Analysis of replicating mitochondrial DNA by two-dimensional agarose gel electrophoresis. *Methods Mol. Biol.*, **372**, 219–232.
44. Vollenweider,H.J., Sogo,J.M. and Koller,T. (1975) A routine method for protein-free spreading of double- and single-stranded nucleic acid molecules. *Proc. Natl. Acad. Sci. U.S.A.*, **72**, 83–87.
45. Sogo,J.M. and Thoma,F. (1989) Electron microscopy of chromatin. *Methods Enzymol.*, **170**, 142–165.
46. Zellweger,R. and Lopes,M. (2018) Dynamic architecture of eukaryotic DNA replication forks in vivo, visualized by electron microscopy. *Methods Mol. Biol.*, **1672**, 261–294.
47. Neelsen,K.J., Chaudhuri,A.R., Follonier,C., Herrador,R. and Lopes,M. (2014) Visualization and interpretation of eukaryotic DNA replication intermediates in vivo by electron microscopy. *Methods Mol. Biol.*, **1094**, 177–208.
48. Sogo,J.M., Ness,P.J., Widmer,R.M., Parish,R.W. and Koller,T. (1984) Psoralen-crosslinking of DNA as a probe for the structure of active nucleolar chromatin. *J. Mol. Biol.*, **178**, 897–919.
49. Giannattasio,M., Zwicky,K., Follonier,C., Foiani,M., Lopes,M. and Branzei,D. (2014) Visualization of recombination-mediated damage bypass by template switching. *Nat. Struct. Mol. Biol.*, **21**, 884–892.
50. Lopes,M., Foiani,M. and Sogo,J.M. (2006) Multiple mechanisms control chromosome integrity after replication fork uncoupling and restart at irreparable UV lesions. *Mol. Cell*, **21**, 15–27.
51. Ramirez,P., Crouch,R.J., Cheung,V.G. and Grunseich,C. (2021) R-loop analysis by Dot-Blot. *J. Vis. Exp.*, **167**, e62069.
52. Sogo,J.M., Portmann,R., Kaufmann,P. and Koller,T. (1975) Adsorption of DNA molecules to different support films. *J. Microsc.*, **104**, 187–198.
53. Dammann,R., Lucchini,R., Koller,T. and Sogo,J.M. (1993) Chromatin structures and transcription of rDNA in yeast Saccharomyces cerevisiae. *Nucleic Acids Res.*, **21**, 2331–2338.
54. DeFrancesco,L. and Attardi,G. (1981) In situ photochemical crosslinking of HeLa cell mitochondrial DNA by a psoralen derivative reveals a protected region near the origin of replication. *Nucleic Acids Res.*, **9**, 6017–6030.
55. Bermudez,I., Garcia-Martinez,J., Perez-Ortin,J.E. and Roca,J. (2010) A method for genome-wide analysis of DNA helical tension by means of psoralen-DNA photobinding. *Nucleic Acids Res.*, **38**, e182.
56. Farge,G. and Falkenberg,M. (2019) Organization of DNA in mammalian mitochondria. *Int. J. Mol. Sci.*, **20**, 2770.
57. Fierro-Fernandez,M., Hernandez,P., Krimer,D.B. and Schvartzman,J.B. (2007) Replication fork reversal occurs spontaneously after digestion but is constrained in supercoiled domains. *J. Biol. Chem.*, **282**, 18190–18196.
58. Smith,S.I. and Brodbelt,J.S. (2010) Rapid characterization of cross-links, mono-adducts, and non-covalent binding of psoralens to deoxyoligonucleotides by LC-UV/ESI-MS and IRMPD mass spectrometry. *Analyst*, **135**, 943–952.
59. Holt,I.J., Kazak,L., Reyes,A. and Wood,S.R. (2016) Analysis of replicating mitochondrial DNA by in organello labeling and two-dimensional agarose gel electrophoresis. *Methods Mol. Biol.*, **1351**, 95–113.
60. Shen,C.K., Hsieh,T.S., Wang,J.C. and Hearst,J.E. (1977) Photochemical cross-linking of DNA-RNA helices by psoralen derivatives. *J. Mol. Biol.*, **116**, 661–679.
61. Bogenhagen,D., Gillum,A.M., Martens,P.A. and Clayton,D.A. (1979) Replication of mouse L-cell mitochondrial DNA. *Cold Spring Harb. Symp. Quant. Biol.*, **43 Pt 1**, 253–262.